OSSI RIEKKINEN

Development and Application of Ultrasound Backscatter Methods for the Diagnostics of Trabecular Bone

Doctoral dissertation

To be presented by permission of the Faculty of Natural and Environmental Sciences of the University of Kuopio for public examination in Auditorium 2, Kuopio University Hospital, on Friday 14th November 2008, at 12 noon

Department of Physics, University of Kuopio
Institute of Biomedicine, Department of Anatomy, University of Kuopio
Department of Clinical Physiology and Nuclear Medicine,
Kuopio University Hospital and University of Kuopio

KUOPION YLIOPISTO

KUOPIO 2008

ABSTRACT

In osteoporosis, changes in tissue structure and composition impair the mechanical strength of bone and increase the risk of fractures. Osteoporosis causes millions of bone fractures annually worldwide. It is commonly diagnosed by means of dual energy X-ray absorptiometry (DXA), a technique that provides information on areal bone mineral density (BMD, g/cm^2). However, most of the low trauma fractures occur in people with normal BMD values.

Quantitative ultrasound (QUS) propagation and scattering depend on both the material and structural properties of bone. Thus, ultrasound measurements provide a method for osteoporosis diagnosis. As ultrasound devices are portable, cheap and do not apply ionizing radiation, they might be suitable for osteoporosis screening.

In the present thesis work, the composition of trabecular bone and its calcified matrix was analysed and compared experimentally, and by using numerical analyses, to ultrasound speed, attenuation and backscattering parameters. In addition, the diagnostic potential of a point-like ultrasound measurement and that of quantitative ultrasound imaging were compared. Further, the effect of overlying soft tissue on the measurement of human trabecular bone was investigated at various ultrasound frequencies. Finally, a novel dual frequency ultrasound technique (DFUS) was evaluated for the soft tissue correction of bone ultrasound measurements.

Bone quantity was the strongest determinant of ultrasound parameters ($r = 0.64$-0.84, $p < 0.01$). Ultrasound backscattering was also significantly related ($r = -0.66$, $p < 0.01$) to the content of calcified matrix collagen. Variation in ultrasound parameter values within the region of interest was seen to relate with the ultimate strength of trabecular bone ($r = -0.82$, $p < 0.01$). Soft tissues overlying the bone induced significant errors (4% - 127%) in the ultrasound measurements. This effect increased with the ultrasound frequency. After correction with the DFUS technique, the magnitude of errors induced by soft tissue on ultrasound backscattering diminished significantly, typically to one tenth.

QUS parameters of trabecular bone are related to both the quantity and quality of trabecular bone. In addition, measurement of the variation in QUS parameters within the area of interest significantly improves the prediction of bone mechanical strength. The present findings together with the novel DFUS method may enable reliable QUS measurements of trabecular bone at various clinically relevant sites. This could have a significant clinical value.

To Hanna and Elviira

ACKNOWLEDGEMENTS

Kuopio, November 2008

Ossi Riekkinen

LIST OF ABBREVIATIONS

AA	average attenuation
AIB	apparent integrated backscattering
BMC	bone mineral content
BMD	bone mineral density
BUA	broadband ultrasound attenuation
BUB	broadband ultrasound backscattering
BV/TV	bone volume fraction
CC_{CM}	calcified matrix collagen content
CT	computed tomography
DA	degree of anisotrophy
DFUS	dual frequency ultrasound
DXA	dual energy X-ray absorptiometry
FDTD	finite difference time domain
FG	femoral groove
FMC	femoral medial condyle
FLC	femoral lateral condyle
GuHCl	guanidine hydrochloride
HCl	hydrogen chloride
IRC	integrated reflection coefficient
MC_{CM}	calcified matrix mineral content
nBUA	normalized broadband ultrasound attenuation
PBS	phosphate buffered saline
PC_{CM}	calcified matrix proteoglycan content
QUS	quantitative ultrasound
ROI	region of interest
SD	standard deviation
SMI	structural model index
SOS	speed of sound
Tb.N.	trabeculae number
Tb.Sp.	trabeculae separation
Tb.Th.	trabeculae thickness
TLP	tibial lateral plateau
TMP	tibial medial plateau
TOF	time of flight
tw	time window
US	ultrasound
vBMD	volumetric bone mineral density

LIST OF SYMBOLS

A area or amplitude
a radius
B absorption due to other relaxation processes
C_p heat capacity at constant pressure
c speed of sound
d diameter
E Young's modulus
F force
f frequency
H the term including ultrasound reflections from different surfaces
h height
I intensity
i imaginary unit
K the correction factor for compensation of ultrasound reflections at the different surfaces
k wave number
m the frequency dependency of H
n number of samples
p pressure or statistical significance
R reflection coefficient
r correlation coefficient
s thickness
T transmission coefficient or temperature
t time
u velocity of medium particle
Z acoustic impedance
x distance or thickness
α attenuation coefficient
α_a absorption coefficient
$\widetilde{\beta}$ fluctuation of compressibility
χ thermal conductivity
Δf effective frequency range
Δt difference of time of flight
γ gas constant
η viscosity
λ wavelength
$\widetilde{\rho}$ fluctuation of density
θ angle

ρ	density
σ_{max}	ultimate strength
ν	Poisson ratio
∇	gradient operator

LIST OF ORIGINAL PUBLICATIONS

This thesis is based on the following original articles referred to by their Roman numerals:

I   Riekkinen O., Hakulinen M.A.,Lammi M., Jurvelin J.S., Kallioniemi A. and Töyräs J., Acoustic properties of trabecular bone-relationships to tissue composition, *Ultrasound in Medicine and Biology* 33:1438-1444, 2007

II   Riekkinen O., Hakulinen M.A.,Töyräs J. and Jurvelin J.S., Spatial variation of acoustic properties is related with mechanical properties of trabecular bone, *Physics in Medicine and Biology* 52:6961-6968, 2007

III   Riekkinen O., Hakulinen M.A.,Timonen M.,Töyräs J. and Jurvelin J.S., Influence of overlying soft tissues on trabecular bone acoustic measurement at various ultrasound frequencies, *Ultrasound in Medicine and Biology* 32:1073-1083, 2006

IV   Riekkinen O., Hakulinen M.A.,Töyräs J. and Jurvelin J.S., Dual frequency ultrasound - New pulse-echo technique for bone densitometry, *Ultrasound in Medicine and Biology* 34:1703-1708, 2008

The original articles have been reproduced with permission of the copyright holders. The thesis also contains previously unpublished data related to paper I.

Introduction

Osteoporosis affects over 200 million individuals worldwide (159). The economic impact of osteoporosis in Europe was about 36 billion euros in 2000 (42). It has been estimated that both number of patients and the economic impact of osteoporosis will further increase along with the aging of the population (113, 143, 147). In osteoporosis, changes in tissue structure and composition impair the mechanical strength of bone and increase the risk of fractures. Thus, early diagnosis of osteoporosis is essential for prevention of fractures. Currently, osteoporosis diagnosis is based on information on areal bone mineral density (BMD) (95), traditionally determined with dual energy X-ray absorptiometry (DXA). Unfortunately, the availability of the DXA devices is low relative to the number of potential patients. Although patients with osteoporotic BMD values (*i.e.* BMD < 2.5 SD below young adult BMD) have a higher risk for fractures than patients with normal BMD values (95–97), most of the low trauma fractures occur in people with normal BMD values (36, 157).

Quantitative ultrasound (QUS) measurements of the heel have been demonstrated to predict osteoporotic fractures with a similar accuracy as BMD (54, 70, 86). As ultrasound propagation and scattering depend on bone structure, composition and mechanical properties (28, 55, 66, 76–78, 125, 129, 170, 175) quantitative ultrasound measurements provide a potential method for osteoporosis diagnosis. Since ultrasound devices are portable and cheap, and use no ionizing radiation, they might be suitable for osteoporosis screening.

The current clinical QUS parameters include the speed of sound (SOS) and the broadband ultrasound attenuation (BUA). The clinical QUS parameters suffer from the uncertainties arising from variable bone size and marrow composition (3, 76, 125, 183). Moreover, soft tissues overlying the bone have a significant impact on the parameters measured (29, 57, 99).

Clinical QUS instruments typically measure the acoustic properties of the calcaneus, which is not a common osteoporotic fracture site (71). In contrast to current clinical through-transmission measurements, backscattering measurements in pulse-echo geometry could more easily enable analyses of common fracture sites, such as the vertebrae, hip and wrist. This could significantly improve the clinical prediction of an individual's susceptibility for bone fracture. Unfortunately, the backscattering

measurements suffer from the uncertainties induced by soft tissue and bone marrow as well (3, 125).

The mechanical properties of trabecular bone depend on its trabecular structure, organic composition and mineral density (24, 119, 132, 168). In osteoporosis, the volume fraction of calcified bone (or BMD) is known to decrease, while the osteoporotic changes in the properties of calcified matrix are not fully understood. However, in certain bone diseases, such as osteogenesis imperfecta, bone collagen is known to be affected and the overall bone strength is decreased (41). QUS may detect decollagenization and diagnose collagen disruption (Ehlers-Danlos syndrome) with more sensitivity than the DXA (31, 78).

Most commercially available ultrasound devices measure acoustic properties at a single point or by scanning an acoustic map of the heel (37, 47, 49, 93, 138, 164). However, the variation in the ultrasound parameters within the region of interest (ROI) and the relation of spatial variation in parameters with the mechanical properties of trabecular bone is poorly known. In addition, as trabecular bone is structurally heterogeneous, the selection of the tissue depth for analysis inside the bone may significantly affect the values of backscattering parameters. However, this issue has not been extensively investigated.

This thesis work investigated the potential of the through-transmission and pulse-echo ultrasound techniques for evaluating the composition of the calcified matrix. The relation between the spatial variation in ultrasound parameters and the bone mechanical strength was also analysed. The effect of tissue depth applied in ultrasound backscattering measurement was also characterized. The effect of overlying soft tissue on acoustic measurements of trabecular bone was examined, and the dual frequency ultrasound technique (DFUS) for minimization of soft tissue effects was introduced. The DFUS technique was initially evaluated using elastomer samples and then validated using human trabecular bone samples overlaid by heterogeneous soft tissue layers.

Properties of trabecular bone

The bony skeleton protects internal organs, and together with ligaments, tendons and muscles it enables locomotion (15, 52, 94, 156). Bone stores various minerals such as calcium, phosphorus, magnesium, sodium and potassium, and blood cells are produced in bone marrow. The human skeleton consists of two types of bone, cortical and trabecular. All the bones in the human skeleton are covered by a cortical bone layer, also called the compact bone layer. The shafts of long bones consist of a cortical bone pipe and a central cavity filled with bone marrow. Trabecular bone can be found in the ends of long bones (*e.g.* femur) and in cuboid bones (*e.g.* calcaneus). Trabecular bone structure is spongy, consisting of calcified matrix and bone marrow (Fig 2.1).
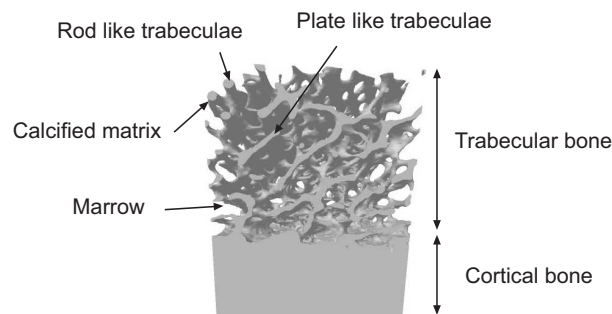
Figure 2.1: The skeleton consists of trabecular and cortical bone. All bones are covered by the cortical bone, while trabecular bone can be found in the internal parts of bones. Trabecular bone consists of calcified matrix *i.e.* trabeculae and marrow-filled pores. The image was acquired from bovine femoral trabecular bone *in vitro* by means of microCT imaging.

2.1 Structure of trabecular bone

The calcified matrix of trabecular bone consists of a network of interconnected trabeculae (154). In the network, the trabeculae are oriented optimally to resist the prevailing loads. The trabeculae may be of various sizes and shapes, such as rods and plates

(Fig. 2.1). The amount and direction of the mechanical stress control the size, shape and orientation of trabeculae. This functional adaptation is described by Wolff's law (182), which states that trabeculae orientate gradually along the direction of the mechanical loading. The structure of trabecular bone can be described with morphometric parameters such as bone volume fraction (BV/TV), trabeculae thickness (Tb.Th.), trabeculae separation (Tb. Sp.), trabeculae number (Tb. N.), the degree of anisotropy (DA) and the structural model index (SMI). These parameters may be determined *e.g.* by means of microCT imaging (72–74, 135, 142). Bone volume fraction is the ratio of calcified matrix volume and total trabecular bone volume. The degree of anisotropy reflects the orientation of the trabeculae, whereas the structural model index indicates their shape whether plate-like or rod-like (Fig. 2.1). Fully isotropic material has a DA value of 1, while the anisotropic structures are described with DA values higher than 1. For a structure constructed ideally of either plates or rods, the SMI value is 0 or 3, respectively. Typical values of morphometric parameters for specific anatomical sites are presented in Table 2.1.

Table 2.1: Morphometric parameters of human trabecular bone at different skeletal sites (33, 44, 58, 100, 124, 144, 149). Extensive variation in the structure between different skeletal sites can be seen.

	BV/TV (%)	Tb.Th. (μm)	Tb.Sp. (μm)	Tb.N (mm^{-1})	DA	SMI
Calcaneus						
Rupprecht *et al.* (149)	0.9 - 39.4	70 - 307	501 - 4010	0.21 - 1.27		
Eckstein *et al.* (44)	14.0 ± 4.9		726 ± 132	1.31 ± 0.19		1.66 ± 0.49
Distal radius						
Pothuaud *et al.* (144)	28.4 ± 4.3	226 ± 18	584 ± 105	1.26 ± 0.17		
Nägele *et al.* (124)	12.0 ± 7.1	148 ± 26	792 ± 113	1.12 ± 0.12	1.88 ± 0.45	2.01 ± 0.82
Proximal femur						
Lai *et al.* (100)	9.0 ± 3.3	123 ± 17	895 ± 128	1.12 ± 0.13	1.78 ± 0.37	1.87 ± 0.45
Pothuaud *et al.* (144)	26.2 ± 6.7	239 ± 23	750 ± 378	1.10 ± 0.25		
Chevalier *et al.* (33)	9.3 - 31.8					
Nägele *et al.* (124)	20.6 ± 12.8	207 ± 57	951 ± 417	1.09 ± 0.33	2.31 ± 0.61	1.01 ± 0.80
Eckstein *et al.* (44)	17.6 ± 9.3	182 ± 46			2.00 ± 0.39	1.27 ± 0.89
Vartebra						
Pothuaud *et al.* (144)	30.6 ± 5.5	233 ± 14	551 ± 139	1.31 ± 0.21		
Nägele *et al.* (124)	10.2 ± 4.1	140 ± 14	986 ± 177	0.99 ± 0.17	1.50 ± 0.29	1.71 ± 0.61
Gong *et al.* (58)	7.5 ± 1.8	113 ± 13		1.17 ± 0.19	1.43 ± 0.17	
Distal tibia						
Lai *et al.* (100)	7.6 ± 4.5	125 ± 30	979 ± 164	1.02 ± 0.15	2.01 ± 0.26	2.25 ± 0.58

BV/TV = bone volume fraction, Tb.Th. = trabeculae thickness, Tb.Sp. = trabeculae separation, Tb.N. = trabeculae number, DA = degree of anisotrophy and SMI = structural model index.

2.2   Composition of trabecular bone

Trabecular bone consists of bone marrow and calcified matrix (15, 52, 94, 156). In the human skeleton, the relative portion of calcified matrix in trabecular bone volume, *i.e.* the bone volume fraction, varies typically between 1% and 40% (33, 44, 58, 100, 124, 144, 149). Calcified matrix consists of two phases, *i.e.* an inorganic and an organic phase; 65-70% and 30-35% of the calcified matrix weight consists of inorganic and organic substances, respectively. The inorganic part consists mainly of hydroxyapatite

$(Ca_{10}(PO_4)_6(OH)_2)$ while the organic part consists of various proteins. The predominant protein is type I collagen, which accounts for 85-90% of the weight of the organic component in the calcified matrix (6)(Fig. 2.2). Typical values for calcified matrix mineral and collagen contents at specific anatomical sites are presented in Table 2.2.
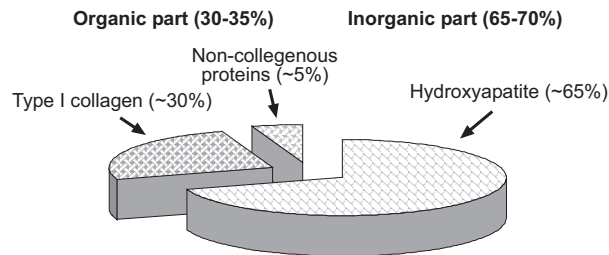
Figure 2.2: Calcified matrix consists of inorganic (mainly hydroxyapatite) and organic (mainly collagen I) parts.

Table 2.2: Mineral (ash) and collagen content of calcified matrix at different human skeletal sites (1, 40). Significant variation in composition can be seen between the sites. Ding *et al.* (1997) (40) assumed that 13.4% of the collagen content is hydroxyproline. This assumption is used to derive the collagen content from the results of the study by Aerssens *et al.* (1997)(1).

	Collagen content (%)	Mineral content (%)
Calcaneus		
Aerssens *et al.* (1)	21.6	60.5
Iliac crest		
Aerssens *et al.* (1)	23.5	59.9
Proximal femur		
Aerssens *et al.* (1)	23.4	61.9
Vertebra		
Aerssens *et al.* (1)	24.9	59.2
Proximal tibia		
Ding *et al.* (40)	25.4	66.4

Almost all (99%) of the calcium in the body is stored in the bones, in the form of calcium hydroxyapatite. With this dynamic calcium storage, the body can regulate the calcium balance in the blood circulation. Collagen I is a highly cross-linked protein (41) with a diameter and length of 50-80 nm and 300 nm, respectively. The tensile strength of collagen fiber is higher even than that of steel (52), and, together with hydroxyapatite, collagen determines the mechanical properties of bone (48, 165).

Most of the bone marrow can be found in the central cavity of long bone shafts and also in pores within the trabecular structure (156). All the marrow cavities of a newborn human contain hemapoietically active red marrow whereas the marrow cavities of an adult also contain yellow marrow, which is mainly fat. The central cavity of long bone shafts of an adult human consists mainly of yellow marrow whereas red marrow can be found in trabecular bone marrow cavities (59).

2.3   Mechanical properties of trabecular bone

Since the skeleton enables locomotion and protects the internal organs, the mechanical properties of bone are important for functionality and wellbeing. The mechanical properties of trabecular bone depend on the structure, composition and quantity of calcified matrix. These properties are strongly affected by the mechanical stresses applied to the bone. According to Wolff's law, the trabeculae orientate gradually along the direction of mechanical loading, so that eventually the trabeculae will be parallel with the prevailing loading direction. This structure is strong when loaded in the direction of the trabeculae but weaker for loads in other directions. The mechanical properties of trabecular bone can be determined *in vitro e.g.* by using tension (4, 26), compression (11, 27, 34, 51, 56, 87, 107, 115, 151, 179) and shear tests (69). With these techniques the mechanical properties are derived by analysing the stress-strain behaviour of the sample under mechanical loading (Fig. 2.3).
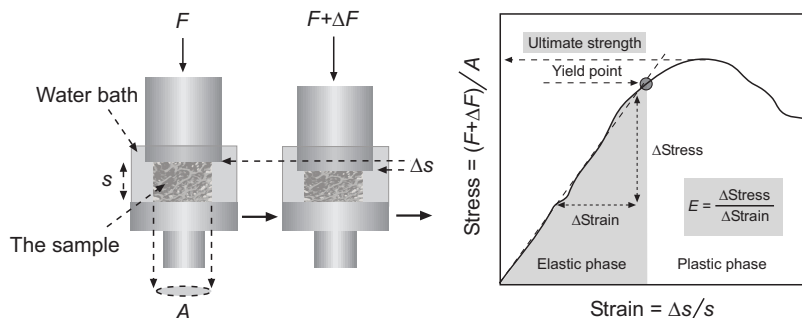
Figure 2.3: A compression test of a trabecular bone sample. The sample is immersed in a saline bath and compressed destructively with a constant strain rate. When the force (F) is normalized by the area of the sample (A), the stress that produces the deformation of the sample (strain) is determined. Finally, the strain is determined by normalizing the deformation of the sample with the original thickness of the sample. During an experiment, the stress and strain are recorded. The Yield point divides the stress-strain curve into elastic and plastic phases. In addition, the area under the stress-strain curve before the Yield point (shaded area) defines the resilience, *i.e.* the energy stored in the sample. Young's modulus (E) is determined as the slope of the linear part of the curve and the ultimate strength (σ_{max}) is determined as the local maximum of the stress.

In the compression test, the compressive stress and deformation (*i.e.* strain) of the sample are recorded. The test may be conducted in confined (27) or unconfined geometry (Fig. 2.3). Typically, the sample is compressed with a constant strain rate and the induced stress is continuously recorded. The result is a stress-strain curve (161) (Fig. 2.3). Mechanical parameters such as Young's modulus (E), ultimate strength (σ_{max}) (161) and strain, yield stress and strain and resilience can be determined from the stress-strain curve. Young's modulus is a measure of the elastic stiffness of trabecular bone. Ultimate strength indicates the stress value where the calcified matrix structure collapses permanently. The yield point divides the stress-strain curve into elastic and plastic phases (Fig. 2.3), *i.e.* the deformation of the trabecular bone sample

is permanent after the Yield point. The area under the stress-strain curve before the Yield point defines the resilience (Fig. 2.3), *i.e.* the energy stored in the sample during the elastic phase. Young's modulus (*E*) is determined as the slope of the linear part of the curve (Fig. 2.3) and ultimate strength is determined as the local maximum stress value (Fig. 2.3). Typical values of Young's modulus and ultimate strength at several anatomical sites of the human skeleton are presented in Table 2.3.

Table 2.3: Mechanical parameters of human trabecular bone at different skeletal sites (23, 67, 118, 127). Extensive variation in mechanical parameters between different skeletal sites can be seen.

	Ultimate strength (MPa)	Young's modulus (MPa)	Orientation
Calcaneus			
Mittra *et al.* (118)	1.9 ± 1.0	70 ± 59	ML
Distal femur			
Burgers *et al.* (23)	3.2 ± 2.1	376 ± 347	AP
Hakulinen *et al.* (67)	10.9 ± 4.2	624 ± 214	SI
Proximal femur			
Schoenfeld *et al.* (151)	0.1 - 13.5		
Proximal tibia			
Hakulinen *et al.* (67)	9.5 ± 3.9	575 ± 179	SI
Vartebra			
Nicholson *et al.* (127)		165 ± 72	SI
Nicholson *et al.* (127)		52 ± 31	AP
Nicholson *et al.* (127)		43 ± 25	ML

ML, medial-lateral; AP, anterior-posterior; SI, superior-inferior

In the compression test, the sample preparation, hydration, temperature and strain rate influence the values of the mechanical parameters of trabecular bone. Misaligned surfaces of the sample can cause underestimation of Young's modulus and ultimate strength (109, 160, 161), whereas dehydration of the sample causes overestimation of the mechanical parameters (110). Young's modulus of bone has been found to be 7% higher at room temperature than at body temperature (21). Therefore, it is important to control the variation of the ambient temperature. Control of the strain rate is important in trabecular bone mechanical testing (27, 108). Trabecular bone consists of solid (calcified matrix) and fluid (marrow) phases, which is characteristic of poroviscoelastic material (108). Because of this property, high strain rates induce hydraulic stiffening of bone, as there is not enough time for the marrow to flow out of the bone. Further, due to the intrinsic viscoelasticity of calcified matrix, both ultimate strength and Young's modulus may increase with strain rate even when the marrow is removed (27).

2.4 Bone changes in osteoporosis

In osteoporosis, bone mass decreases and the calcified matrix structure deteriorates. Three bone cell types are responsible for the variation in bone mass: osteoblasts, osteocytes and osteoclasts (15, 52, 94, 156). Osteoblasts produce osteons and help them to mineralize, whereas the osteoclasts dissolve the mineralized osteons. Osteocytes are osteoblasts which have drifted into mineralized bone. It is thought that osteocytes

play an active role in bone turnover but the function of osteocytes is not fully understood (122). However, the osteoclasts are more active than the osteoblasts in bone turnover in osteoporosis. As the osteoclasts and osteoblasts act at the bone surface, this is the area where the bone turnover takes place. Although 80% of the skeleton mass consists of cortical bone, the surface of cortical bone covers only 20% of the total bone surface within the skeleton. Because of this, trabecular bone is renewed about eight times faster than cortical bone (141, 154). For this reason, measurement of the properties of trabecular bone is thought to be essential in osteoporosis diagnosis.

In osteoporosis, the cortical bone layer becomes thinner and trabecular bone structure becomes more sparse. Furthermore, the thickness and connectivity of trabeculae decrease and the separation of trabeculae increases (7) (Table 2.4). As a consequence, the bone volume fraction and the mechanical strength decrease.

Table 2.4: Morphometric properties of healthy and osteoporotic trabecular bone at different skeletal sites (18, 80, 122, 153).

		BV/TV (%)	Tb.Th. (μm)	Tb.Sp. (μm)	Tb.N. (mm^{-1})
Vartebra					
Homminga *et al.* (80)	Healthy	14	268	957	0.99
Homminga *et al.* (80)	Osteoporotic	10	238	1111	0.87
Iliac crest					
Mullender *et al.* (122)	Healthy	23	138	479	1.66
Mullender *et al.* (122)	Osteoporotic	14	117	790	1.19
Shahtaheri *et al.* (153)	Healthy	25	121		0.48
Shahtaheri *et al.* (153)	Osteoporotic	10	96		0.11
Distal radius					
Boutroy *et al.* (18)	Healthy	13	78	517	1.71
Boutroy *et al.* (18)	Osteoporotic	9	63	714	1.32
Distal tibia					
Boutroy *et al.* (18)	Healthy	14	89	551	1.60
Boutroy *et al.* (18)	Osteoporotic	10	77	750	1.27

BV/TV = bone volume fraction, Tb.Th. = trabeculae thickness, Tb.Sp. = trabeculae seperation and Tb.N. = trabeculae number.

Bone diagnostics with ultrasound

3.1 Basic physics of ultrasound

Ultrasound is defined as a propagating mechanical wave with a frequency of over 20 kHz. Sound waves can be divided into transverse, longitudinal, surface and plate wave modes. However, only the longitudinal wave mode is considered in the present studies. In a transverse wave, particles of the medium vibrate perpendicularly to the travelling direction of the wave, whereas in a longitudinal wave the particles vibrate in parallel with the wave direction. The sound wave can be described in three dimensions using the wave equation (75)

$$\nabla^2 p - \frac{1}{c^2}\frac{\partial^2 p}{\partial t^2} = \frac{1}{c^2}\widetilde{\beta}\frac{\partial^2 p}{\partial t^2} + \nabla \cdot [\widetilde{\rho}\nabla p], \tag{3.1}$$

where ∇ is the gradient operator, c the average sound speed in medium, p the sound pressure, t the time, $\widetilde{\beta}$ the fluctuation of compressibility and $\widetilde{\rho}$ is the fluctuation of density of the medium. With an assumption that the medium exhibits constant compressibility and density, equation 3.1 can be written as follows (75):

$$\nabla^2 p - \frac{1}{c^2}\frac{\partial^2 p}{\partial t^2} = 0. \tag{3.2}$$

By simplifying the presentation from three dimensions to one, a solution for the partial differential equation 3.2 can be expressed as follows (43, 75):

$$p(x,t) = Ae^{ik(x-ct)}, \tag{3.3}$$

where x is distance, A is the amplitude, k the wave number and i the imaginary unit. Newton's second law can be written as follows (75):

$$\frac{\partial u}{\partial t} = -\frac{1}{\rho}\nabla p, \tag{3.4}$$

where u is the velocity of medium particles and ρ the density of the medium. The velocity of medium particles u can be solved from equations 3.3 and 3.4 as follows:

$$u(x,t) = \int -\frac{1}{\rho}\frac{\partial Ae^{ik(x-ct)}}{\partial x}dt = \frac{1}{c\rho}Ae^{ik(x-ct)}. \tag{3.5}$$

Acoustic impedance Z is the ratio of pressure p and particle velocity u (14, 75, 181). For the plane wave, the acoustic impedance can be solved from equations 3.3 and 3.5 as follows:

$$Z = \frac{Ae^{ik(x-ct)}}{\frac{1}{c\rho}Ae^{ik(x-ct)}} = \rho c. \tag{3.6}$$

Table 3.1: An ultrasound wave is reflected at the interface of two acoustically different materials. The amplitude of the reflected wave depends on the difference between the acoustic impedances of the materials (75). The speed of sound in isotropic solid material depends on the mechanical properties and density of the material (180).

Parameter	Equation
Reflection coefficient	$R = \left(\frac{Z_2 cos\theta_1 - Z_1 cos\theta_2}{Z_2 cos\theta_1 + Z_1 cos\theta_2}\right)^2$
Transmission coefficient	$T = \frac{4Z_1 Z_2 cos\theta_1 cos\theta_2}{(Z_2 cos\theta_1 + Z_1 cos\theta_2)^2}$
Sound speed in isotropic solid	$c = \sqrt{\frac{E(1-\nu)}{\rho(1+\nu)(1-2\nu)}}$
Pressure field	$p(x,t) = Ae^{ik(x-ct)}e^{x\alpha}$

Z = acoustic impedance, A = amplitude, E = Young's modulus, ν = Poisson's ratio, ρ = density, i = imaginary unit, k = wave number, x = distance, t = time and α = attenuation coefficient. θ_1 and θ_2 are the angles of the incidence and refraction, respectively. Subscripts 1 and 2 refer to the first and second medium.

When the ultrasound wave travels through the medium, it is attenuated (43, 75) (Table 3.1). The main causes of attenuation are scattering, reflection and absorption (180). Scattering is due to elastic discontinuities (*i.e.* scatterers) in a medium. Ultrasound scattering can be divided into three categories based on sound wavelength. The scattering phenomenon is different when the ultrasound wavelength is shorter than, the same as, or greater than the size of the scatterers in the medium (181). When the wavelength is shorter than the scatterer dimensions, the scattering can be described as a reflection phenomenon. When the wavelength is the same as the dimensions of the scatterer, the scattered sound field has a complex distribution and is sensitive to changes in scatterer dimensions and acoustic impedances (45). When the wavelength is much greater than the scatterer, the scattered sound field is uniformly distributed. For example, with spherical scatterers the intensity of scattering sound (*I*) is proportional to wavelength λ and the radius of the scatterer (*a*) as follows (181):

$$I \propto \frac{a^6}{\lambda^4} \tag{3.7}$$

In absorption, the energy of the mechanical ultrasound wave is dissipated as heat and in other forms of energy through heat conduction, viscous relaxation and some other relaxation processes (75, 181). Absorption (α_a) can be described mathematically as follows (75, 92):

$$\alpha_a(f,T) = \frac{4\pi^2 f^2}{\rho c^3} \left[\frac{4\eta}{3} + \frac{(\gamma - 1)\chi}{C_p} \right] + \sum_j B(f,T) \tag{3.8}$$

where f is the ultrasound frequency, T the temperature of the medium, ρ the density of the medium, c the sound speed in the medium, η the viscosity, γ the gas constant, χ the thermal conductivity, C_p the heat capacity at constant pressure, and B the absorption due to other relaxation processes.

3.2 Quantitative ultrasound methods in osteoporosis diagnosis

The first studies on the ultrasonic determination of the mechanical properties of trabecular and cortical bone date back to the 1970s (102, 186). At that time, the interest was in basic ultrasound research. In the 1980s, interest in using ultrasound for osteoporosis diagnosis increased rapidly. Christian Langton's study on the ultrasound attenuation in the calcaneus (104) initiated a new field in osteoporosis diagnosis.

3.2.1 Clinical methods

Clinical ultrasound devices designed for osteoporosis diagnosis can make measurements of peripheral skeletal sites such as the calcaneus (35, 50, 53, 54, 70, 86, 88, 93, 117, 134, 148, 164) radius (8, 20, 35, 158) and phalanxes (2, 8, 35, 54, 158). The peripheral sites are easily reachable since the thickness of the disturbing soft tissue layer overlying the bone is smaller than at central skeletal sites such as the lumbar spine and proximal femur.

Current clinical methods can be divided into through-transmission and axial-transmission techniques (133). The most common clinical approach has been the measurement of the acoustic properties of the heel using the through-transmission technique (Fig. 3.1). With this technique, ultrasound attenuation and speed through the heel are determined. Two measurement techniques have been commonly applied: *i.e.* substitution (104) and contact techniques (3). In the substitution technique, the time of flight and the frequency spectrum of an ultrasound pulse are measured through the water bath with and without the heel. The difference in the time of flight through the water bath with and without the heel is used in the calculation of the sound speed (Table 3.2). The ultrasound attenuation spectrum can be determined by comparing the frequency spectra of the ultrasound pressure amplitude measured through the water bath with and without the heel. The broadband ultrasound attenuation (BUA) is determined as the slope of the linear part of the attenuation spectrum (Table 3.2). In the

contact method, ultrasound transducers are located on the skin surface and coupled with acoustic gel. The ultrasound signal measured through the heel is compared with a reference signal measured through the phantom for determination of speed and attenuation. The sound speed is calculated by comparing the distance of transducers and the time of flight through the heel (Table 3.2). The BUA is calculated similarly as in the substitution technique, although the reference spectrum is determined through a phantom.

Although the heel measurement is a relatively simple ultrasound technique, there are several sources for uncertainty in the technique. The size of the calcaneus (30, 162, 183) and the amount of overlying soft tissue (29, 57, 90, 99) are significant error sources which might affect the measurement. Some devices using the substitution technique assume constant thickness of bone for all subjects, which inevitably induces inaccuracy in the calculated ultrasound parameters (Table 3.2). Further, the size of the foot may introduce variations in the values of the ultrasound measurement (37, 39, 163, 164) because the anatomical locations of the acoustic measurement for small and large feet may not be identical. This error source can be minimized using imaging devices with which the region of interest in the calcaneus can be accurately located. Furthermore, as the composition of the overlying soft tissue may vary, it can affect the measurements. This is important, since the current clinical ultrasound devices do not take into account the variation in thickness and composition of overlying soft tissue.

The through-transmission technique   The axial-transmission technique

a)   Water bath   b)
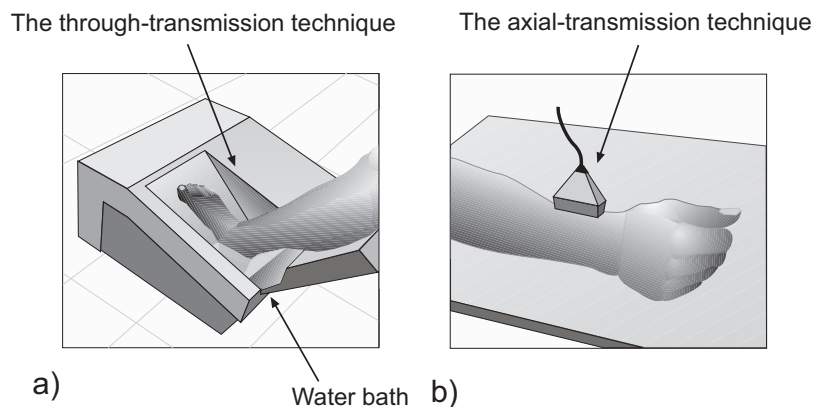
Figure 3.1: Clinical ultrasound devices designed for osteoporosis diagnosis are based on through-transmission or axial-transmission techniques. (a) The through-transmission technique is suitable for the measurement of peripheral trabecular bones such as the heel bone. (b) The axial-transmission technique is used for evaluation of the acoustic properties of cortical bone *e.g.* in the radius.

In the axial-transmission technique (Fig. 3.1), both ultrasound transducers are located on the same side of the bone. With this technique, the speed of sound on the surface of cortical bone (Table 3.2) can be measured at various locations. For example, the acoustic properties of the radius and phalanxes can be measured. As the speed of ultrasound propagation in the cortical bone layer depends on the elastic properties,

porosity and geometrical properties of the cortical bone, this technique can provide clinically valuable information (17, 123, 145). Soft tissues overlying the bone affect the values of sound speed and only peripheral sites can be measured reliably.

Table 3.2: Basic ultrasound equations used in the determination of the ultrasound parameters of bone in clinical ultrasound devices.

Technique	Parameter	Equation
Substitution	Speed of Sound	$\dfrac{c_w s_h}{s_h - (\Delta t c_w)}$
Contact	Limb Velocity	$\dfrac{s_h}{t_h}$
Axial	Ultrasound Velocity	$\dfrac{s}{t}$
Substitution and Contact	Ultrasound attenuation spectrum*	$8.686(\ln(\frac{A_w(f)}{A_b(f)}) + \ln(T_{sb}T_{bs}))$

c_w = sound speed in water, s_h = thickness of the heel, Δt = time of flight difference through the water bath with and without the heel, t_h = time of flight through the heel, s = distance between the ultrasound transducers, t = time of flight between the ultrasound transducers, A_b and A_w = ultrasound pressure amplitude spectra measured through the water bath with and without the heel, respectively. T = transmission coefficient. Subscripts sb and bs refer to soft tissue-bone and bone-soft tissue interfaces, respectively.

*Broadband Ultrasound Attenuation (BUA) is determined as the slope of the linear part of the attenuation spectrum.

3.2.2 Potential ultrasound methods for diagnosis

Fractures in the lumbar spine and proximal femur may be most accurately predicted when the bone properties are measured directly at the fracture sites, not at the peripheral sites (19, 114). Thus, current clinical ultrasound devices which are capable of only peripheral measurements are not optimal for the prediction of osteoporotic fractures at central sites. Consequently, there is increasing interest in the possibility of ultrasound measurements of central skeletal sites (9, 10, 38, 60, 62, 63, 126, 138).

The acoustic properties of the proximal femur have been measured with the through-transmission technique *in vitro* (10, 38, 60, 62, 63, 138) and *in vivo* (9). In these studies, ultrasound was successfully applied for parametric imaging of the human proximal femur. The speed of sound and broadband ultrasound attenuation in the proximal femur were found to be significant predictors of bone mineral density. Further, Nicholson *et al.* (2007)(126) measured the acoustic properties of the vertebra lumbalis by using the through-transmission technique and compared those with the mechanical properties of the samples. In that study, ultrasound speed and attenuation were found to be significant predictors of failure load of the vertebrae.

An alternative to through-transmission and axial-transmission methods is the pulse-echo ultrasound technique (Fig. 3.2). In this technique, only one ultrasound transducer is used for the measurement of ultrasound scattering and reflection. The reflec-

tion and backscattering parameters have been shown to relate with the mechanical properties, structure and mineral density of trabecular bone (28, 66–68, 77, 125, 175, 176, 178). There is also some evidence that by using the pulse-echo technique it is possible to measure the thickness of the cortical bone layer in long bone shafts (98, 172) with comparable accuracy to peripheral quantitative computed tomography (98). Advantageously, the pulse-echo measurements may be conducted at typical fracture sites that are not readily accessible by trough-transmission techniques.

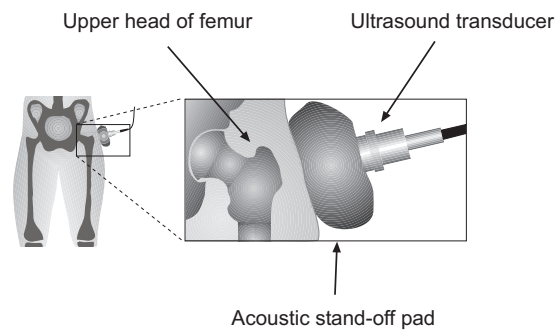**Figure 3.2:** Pulse-echo ultrasound measurement of the trochanter major. This kind of *in vivo* measurement set-up is used for measurement of the calcaneus (174) and preliminary trochanter major (in the our laboratory in 2008). Reflection and backscattering of ultrasound from the trochanter major may predict hip fractures. An acoustic stand-off pad may be used to focus the ultrasound beam on the surface of the bone.

Models of
the acoustic properties of trabecular bone

4.1 Analytical models

Quantitative ultrasound measurements of trabecular bone have been in use for over 20 years. However, the relationships between the ultrasound propagation and the structural, compositional and mechanical properties of trabecular bone are not fully understood. Modelling ultrasound propagation through bone tissue provides tools for understanding the interaction between ultrasound and trabecular bone.

Biot's theory, traditionally used in geophysical applications, has been applied in modelling ultrasound propagation through trabecular bone (46, 65, 85, 105, 152, 177). Biot's theory considers the propagation of longitudinal and transverse elastic waves in porous solids (12, 13) by assuming that the medium is isotropic and scattering is negligible. As input Biot's theory requires 14 different parameters for the wave calculations. For example, material parameters such as densities of calcified matrix and marrow, Young's modulus for calcified matrix and bulk modulus for marrow are required (46, 65, 85, 105). Moreover, specific structural parameters, such as porosity and the sample pore size must be known. Some of the input parameters are difficult to determine experimentally, so the application of Biot's theory is rather difficult in the case of trabecular bone. However, when applied successfully, Biot's theory has been found to predict the propagation of fast and slow compressive waves in trabecular bone, which has been verified in experimental studies (83).

Schoenberg's theory of ultrasound propagation in a periodic stratified medium assumes that the medium is layered (84, 85, 106, 171). When modelling ultrasound propagation in a trabecular bone layered medium, the assumption is valid only for a plate-like trabecular bone structure (84, 85, 106). Schoenberg's theory needs only six input parameters for wave calculations: the densities of calcified matrix and marrow, porosity, speed of the longitudinal wave in calcified matrix and marrow, and speed of the transverse wave in calcified matrix. Schoenberg's theory has been reported to predict the dependence of the phase velocity of a fast wave with trabecular orientation (84). It has also been shown to predict the slow wave when ultrasound propagates in parallel with the orientation of plate-like trabeculae (84). Importantly, Schoenberg's

theory can predict the positive linear relation between ultrasound attenuation and frequency (106).

Biot's and Schoenberg's theories have been used to model ultrasound propagation in trabecular bone. There are also models for ultrasound backscattering inside the trabecular bone (89, 130, 140, 169). Wear (1999) used the theory for acoustic wave scattering from solid cylinders to model ultrasound backscattering in trabelular bone. Jenson *et al.* (2003) used autocorrelation functions to compute the ultrasound backscattering coefficient for human trabecular bone. These studies reported an agreement between the experimental backscattering measurements and the model prediction of frequency dependence of backscattering (89, 169). The ultrasound model developed for scattering in soft tissues may also be applied for trabecular bone (130). In this model, scattering is assumed to depend on the sound speed fluctuation between bone and marrow. Nicholson *et al.* (2000) applied this model and showed that the acoustic properties of trabecular bone were affected by bone structure (size of scatterers) independently of bone volume fraction.

4.2   Numerical models

Analytical models are generally applicable when the structure of the medium is homogenous, isotropic or otherwise periodical. However, the structure of trabecular bone is more complicated and varies typically with bone volume fraction; the structure of dense bone is more plate-like than that of porous bone (72, 100). Numerical models combine acoustic theories (wave equation) and complicated trabecular bone structure (81, 82). Real trabecular bone structure, obtained using the microCT technique, is used as a basis for the numerical model (61, 64, 112, 139). In these models, the wave equation is solved using numerical techniques, for example using the finite-difference time-domain (FDTD) algorithm (61, 64, 81, 82, 139). This makes it possible to study the interactions between the ultrasound and bone structure and composition. Since it is complicated or even impossible to solve the detailed interactions of the structure and composition of calcified matrix on ultrasound speed, attenuation and scattering with experimental studies, numerical simulations play an important role in bone ultrasound research.

Hosokawa (2006) found that an FDTD model extended with Biot's theory can predict both fast and slow waves when ultrasound propagates through the trabecular bone in a direction parallel to the trabeculae orientation in a 2D structure (82). Hosokawa also found that the model predicted the amplitude ratio of fast and slow waves more precisely than the analytical Biot's theory did (81). Padilla *et al.* (2006)(139) investigated the numerical simulation of ultrasound propagation in 3D trabecular bone geometry (61, 64, 139). They found, in agreement with the experiments, that an increase in ultrasound speed and attenuation is positively related with the bone volume fraction. Furthermore, they also observed the fast and slow waves when ultrasound propagated through trabecular bone in a direction parallel to the orientation of the trabeculae. With these 3D simulation techniques it is possible to evaluate the effect of the quality and quantity of calcified matrix on ultrasound propagation

and scattering. Haiat et al. (2006 and 2007) have investigated this issue and report that the quantity (*i.e.* volume fraction) significantly affects the ultrasound parameters, whereas the quality (*i.e.* properties of trabeculae) has only a minor affect (61, 64).

Aims of the present study

Clinical ultrasound measurements can predict future bone fractures with moderate accuracy. Typically, clinical measurements are conducted in the heel using the through-transmission technique. Unfortunately, the typical osteoporotic fracture sites, *i.e.* the vertebra and proximal femur, are not accessible with current clinical ultrasound techniques. Further, the effect of soft tissues overlying the bone on bone ultrasound measurements is not controlled. Moreover, the optimal ultrasound frequency and the region of interest to predict the mechanical properties of trabecular bone are still unknown.

The aims of the present study were:

1. To investigate the relationships of ultrasound parameters with the composition and mechanical properties of trabecular bone

2. To compare the feasibility of a single value, spatial variation and mean value of ultrasound parameters within the region of interest to predict the mechanical properties of trabecular bone

3. To clarify, at various ultrasound frequencies, the effects of overlying soft tissues on the acoustic parameters of trabecular bone

4. To develop a novel method for minimizing the effects of soft tissues on bone ultrasound measurements

Materials and methods

This thesis work consists of four independent Studies (I - IV). In this section the materials and methods used in the Studies are summarized.

6.1 Materials

The material investigated in Studies I - IV is summarized in Table 6.1. Human trabecular bone specimens were investigated in all Studies. Porcine soft tissues and elastomer samples were also investigated in Studies III and IV.

Table 6.1: Summary of materials investigated in Studies I - IV.

Study	Materials	n	Geometry	Size	Site
I	Human trabecular bone	26	Cylindrical samples	d = 16 mm h = 8 mm	FMC TMP FG
II	Human trabecular bone	20	Cylindrical samples	d = 16 mm h = 8 mm	FMC TMP
III	Human trabecular bone	25	Cylindrical samples	d = 16 mm h = 7.5 mm	FLC TLP
	Porcine adipose and lean tissue	25	Cylindrical samples	d = 48 mm h = 10 - 20 mm	-
IV	Elastomer	6	Cylindrical samples	d = 15 - 26 mm h = 4 - 10 mm	-
	Human trabecular bone	25	Cylindrical samples	d = 16 mm h = 7.5 mm	FLC TLP
	Porcine lean tissue	25	Cylindrical samples	d = 48 mm h = 10 - 20 mm	-

FMC = femoral medial condyle, TMP = tibial medial plateu, FG = femoral groove, FLC = femoral lateral condyle and TLP = tibial lateral plateu.
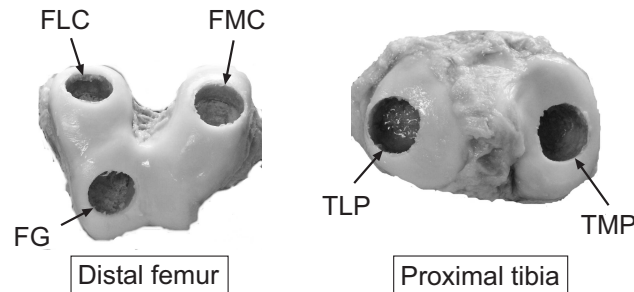
Figure 6.1: The anatomical sites of the human trabecular bone samples investigated in Studies I - IV.

6.1.1 Human samples

In Studies I - IV, human trabecular bone samples were collected from cadaver knees (n = 13, Figure 6.1) with the permission of the National Authority of Medicolegal Affairs (Helsinki, Finland, permission 1781/32/200/01). In Studies I and II, cylindrical plugs of trabecular bone were drilled from the medial femoral condyle, femoral groove and tibial plateau (n = 20 - 26), whereas in Studies III and IV the samples were drilled from the lateral femoral condyle (n = 13) and lateral tibial plateau (n = 12), using a hollow drill bit. The sample surfaces were cut so as to be parallel using a low speed diamond saw (Buehler Isomet Low Speed Saw, Buehler Ltd., Lake Bluff, IL, USA) and the EXACT micro-grinding system (Macro Exact 310 CP, EXACT Apparatebau GmbH & Co., Norderstedt, Germany). Subsequently, the samples were immersed in phosphate buffered saline (PBS) and stored in a freezer (-20°C) until measurement.

6.1.2 Porcine samples

In Studies III and IV, cylindrical soft tissue disks were prepared just before measurement from fresh porcine adipose (n = 25, fat content 70%) and lean (n = 25, fat content 4%) tissues provided by the local slaughterhouse (Atria Oy, Kuopio, Finland). The disks (diameter = 48 mm, thickness = 1 - 2 cm) were prepared using a custom-made biopsy punch (diameter = 48 mm). In addition, the typical composition of human soft tissue was mimicked in backscatter and reflection measurements using porcine lean tissue (n = 25) with a fat content of 30%.

6.1.3 Elastomer samples

In Study IV, the acoustic properties of three elastomers (3a-c, Teknikum Oy, Vammala, Finland, diameter = 26 mm) were analysed. The thickness of the elastomers 3a, 3b and 3c were 10.25 mm, 5.50 mm and 6.00 mm, respectively (x_3 in Figure 6.3, diameter = 16 mm). The elastomers 3a-c (Figure 6.3) were measured with and without the overlying elastomers 1 and 2 (RAPRA Technology Ltd, Shropshire, UK) (Figure 6.3). Three

interfering layers were constructed by applying different thicknesses for elastomers 1 and 2 (x_1 and x_2 in Figure 6.3, respectively), *i.e.* 1.19 mm and 3.22 mm (combination 1), 2.00 mm and 1.85 mm (combination 2) and 3.01 mm and 0.97 mm (combination 3), respectively. Thus, the elastomers 3a, 3b and 3c were measured with three different combinations (1-3) of overlying interfering elastomers.

6.2 Methods

The methodology used in Studies I-IV is summarized in Table 6.2

Table 6.2: Summary of the methods applied in Studies I - IV.

Study	Methods	Device	Parameters	Voltage/Frequency
I	QUS	UltraPAC	nBUA, SOS, AA, BUB, IRC	2.25 MHz
	microCT	SkyScan 1072	BV/TV	80 kV
	Biochemical assay	-	Water content, fat content, CC_{CM}, PC_{CM}	-
	DXA	Lunar Prodigy	BMD	76 kV (K-edge filter)
II	QUS	UltraPAC	nBUA, SOS, AA, AIB, IRC	2.25 MHz
	Mechanical testing	Zwick 1484	σ_{max}	-
III	QUS	Optel	nBUA, SOS, AA, BUB, IRC	0.5 MHz, 1.0 MHz, 2.25 MHz, 3.5 MHz, 5.0MHz
	DXA	Lunar Prodigy	BMD	76 kV (K-edge filter)
	Mechanical testing	Instron 8874	E, σ_{max}	-
IV	QUS	Optel	BUB, IRC	2.25 MHz, 5.0 MHz
		UltraPAC	SOS, AA, IRC	2.25 MHz, 5.0 MHz

QUS = quantitative ultrasound, nBUA = normalized broadband ultrasound attenuation, SOS = speed of sound, AA = average attenuation, BUB = broadband ultrasound backscattering, IRC = integrated reflection coefficient, BV/TV = bone volume fraction, CC_{CM} = calcified matrix collagen content, PC_{CM} = calcified matrix proteglycan content, BMD = bone mineral density, DXA = dual energy X-ray absorptiometry, AIB = apparent integrated backscattering, σ_{max} = ultimate strength and E = Young's modulus.

6.2.1 Experimental ultrasound methods

In Studies I, II and IV, acoustic measurements were conducted with an ultrasound system (UltraPAC, Physical Acoustic Co., NJ, USA) consisting of a 500 MHz A/D-board and a 0.2 - 100 MHz pulser-receiver board. In Studies III and IV, ultrasound measurements were conducted with the Opbox-01/100 (Optel Ltd., Wroclaw, Poland) portable ultrasound instrument. The resolution and sampling frequency of the A/D converter were 8 bits and 100 MHz, respectively. The pulser-receiver bandwidth (-6 dB) was 0.1 - 25 MHz. In Studies I and II, the UltraPAC ultrasound system was equipped with a tank and scanning drives (Fig 6.2 a), whereas in Studies III and IV a custom measurement set-up was constructed for ultrasound measurements (Fig. 6.2 b). In Studies I and II, the measurements were conducted using a single pair of ultrasound transducers (2.25 MHz) whereas in Study III five pairs of ultrasound transducers (Panametrics Inc., Waltham, MA, USA) with different focal properties and centre frequencies (0.5

MHz, 1.0 MHz, 2.25 MHz, 3.5 MHz and 5.0 MHz) were used. In Study IV, the measurements were conducted using two pairs of ultrasound tranducers (2.25 MHz and 5.0 MHz). In Studies I and II, the measurements were performed in a scanning mode (scan area of 16 mm $\times$ 16 mm, step size 0.5 mm), whereas in Studies III and IV the measurements were conducted at a single point within the sample. Prior to ultrasound measurement, bone and soft tissue samples were degassed in PBS. All measurements were conducted in a degassed temperature-controlled (TES 1310 TYPEK, TES Electrical Electronic Corp., Taipei, Taiwan) water bath. Custom LabVIEW (version 6.1, National Instrument, Austin, Texas, USA) measurement and analysis programs were developed for each study.

PULSE-ECHO MEASUREMENTS

In Studies I - IV, echo signals recorded from the samples were compared with the echo signal recorded from the reference surface (a polished steel plate). All pulse-echo parameters were analysed within the effective frequency range of each transducer (0.3-0.7 MHz, 0.7-1.5 MHz, 1.5-3.8 MHz, 2.0-5.5 MHz and 3.2-6.7 MHz for transducers with centre frequencies of 0.5 MHz, 1.0 MHz, 2.25 MHz, 3.5 MHz and 5.0 MHz, respectively). In Studies I, III and IV, IRC (32) and BUB (148) were determined whereas in Study II AIB (32) was derived with the reference method (Table 6.3). In addition, to investigate the effect of signal windowing, the AIB was analysed using five different time window lengths from 1 to 5 μs with 1 microsecond steps. The BUB was determined from the AIB by compensating the AIB value with the ultrasound attenuation within the sample. The attenuation compensation was determined by using an approximation (Nicholson and Bouxsein 2002) (125) of a more complex compensation term (O'Donnell and Miller 1981) (136). The sample specific attenuation and SOS values determined with the through-transmission technique were used in the attenuation correction (125). In Studies I and II, acoustic parameters were calculated as a mean value within a circular ROI (88 mm^2, the total number of the pixels was 352). In addition, in Study II standard deviations of the parameters within the ROI were analysed. In Studies III and IV, acoustic parameters were determined at a single measurement point.

THROUGH-TRANSMISSION MEASUREMENTS

In Studies I - III, speed of sound (SOS), normalized BUA (nBUA) and average attenuation (AA) were determined with the substitution method (104) (Table 6.3). In Study IV, only SOS and AA were determined. SOS was determined with the time of flight (TOF) method (131). TOF was analysed from the radio frequency signal using the threshold technique (128) with a 20% threshold value. AA was determined from the effective range of each transducer, whereas nBUA was calculated as a slope of the linear part of the attenuation spectrum normalized with the sample thickness. The linear part of the attenuation spectrum was defined as a part where the linear correlation coefficient between the attenuation coefficient and the frequency was > 0.9. In Studies I and II, the nBUA was determined using the frequency range of 0.3 - 0.6 MHz, 0.7 -
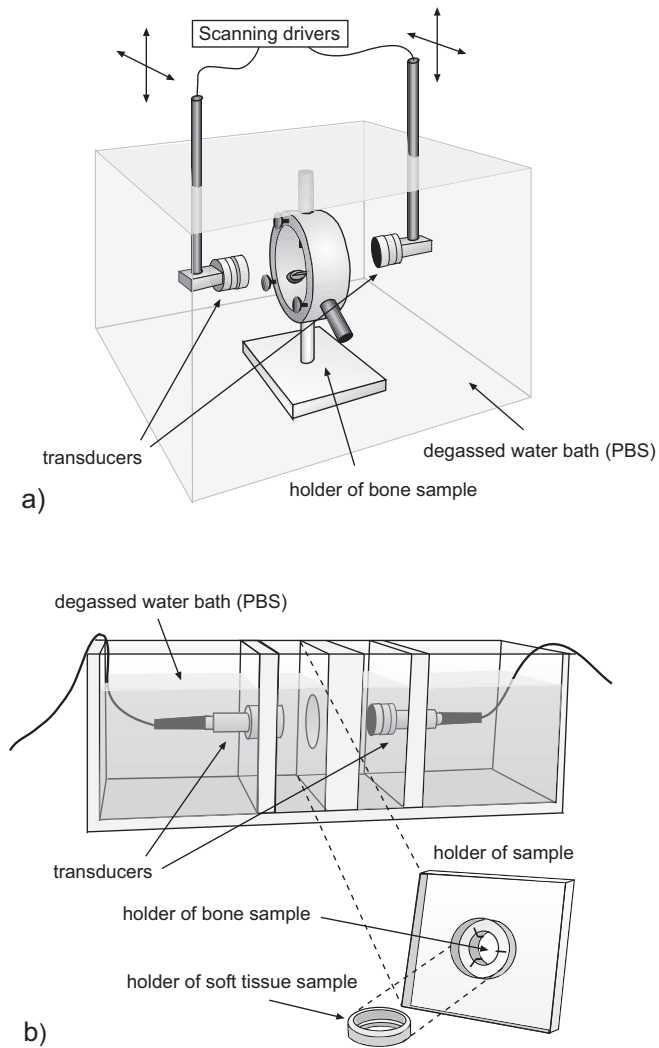
Figure 6.2: The experimental set-up for acoustic measurements applied in Studies I-IV. (a) In Studies I and II, the trabecular bone samples were acoustically imaged (scan area of 16 mm × 16 mm, step size 0.5 mm). (b) In Studies III and IV, the trabecular bone samples were placed in the focal plane of the transducers positioned on opposite sides of the sample and the ultrasound measurements were conducted at a single point. The sample holder stabilized the soft tissues on both sides of the specimen.

Table 6.3: The mathematical definitions of ultrasound parameters determined in Studies I - IV.

Technique	Parameter	Equation
Substitution	SOS	$\dfrac{c_w s}{s - (\Delta t c_w)}$
Substitution	Attenuation*	$\frac{8.686}{s}(\ln(\frac{A_w(f)}{A_b(f)}) + \ln(T_{ws}T_{sw}))$
Substitution	AA	$\frac{8.686}{s\Delta f}\int_{\Delta f}(\ln(\frac{A_w(f)}{A_s(f)}) + \ln(T_{ws}T_{sw}))$
Reference	IRC	$\frac{8.686}{\Delta f}\int_{\Delta f}\ln(\frac{A_n(f)}{A_r(f)})$
Reference	AIB	$\frac{8.686}{\Delta f}\int_{\Delta f}\ln(\frac{A_b(f)}{A_r(f)})$
Reference	BUB	$\frac{8.686}{\Delta f}\int_{\Delta f}(\ln(\frac{A_b(f)}{A_r(f)}) + \frac{\alpha_b(f)c_b tw}{2})$

c_w = sound speed in water, s = thickness of the sample, Δt = time of flight difference through the water bath with and without the sample, A_b and A_w = ultrasound pressure amplitude spectra measured through the water bath with and without the sample, respectively. T = transmission coefficient calculated based on the measured ultrasound reflection coefficient at the surface of the sample. Subscripts ws and sw refer to water-sample and sample-water interfaces, respectively. Δf = effective frequency range, A_n and A_r = ultrasound pressure amplitude spectra analysed from the echo signal from the sample surface and the reference, respectively. A_b = ultrasound pressure amplitude spectra of the echo signal (backscattering) from the inner structure of the sample. α_b = attenuation coefficient of the sample, c_b = sound speed in the sample and tw = time window length for the determination of backscattering.

*normalized Broadband Ultrasound Attenuation (nBUA) is determined as a slope of the linear part of attenuation spectrum normalized with the sample thickness.

1.5 MHz, 1.0 - 2.8 MHz, 1.0 - 3.0 MHz and 1.5 - 3.0 MHz for the center frequency of 0.5 MHz, 1.0 MHz, 2.25 MHz, 3.5 MHz and 5.0 MHz, respectively. In Study III, the nBUA was calculated using the frequency range of 0.2 - 0.5 MHz, 0.7 - 1.5 MHz, 0.5 - 2.0 MHz, 0.5 - 2.0 MHz and 1.0 - 4.0 MHz for the center frequency of 0.5 MHz, 1.0 MHz, 2.25 MHz, 3.5 MHz and 5.0 MHz, respectively.

6.2.2   Ultrasound analysis of overlying soft tissues

In Study III, the trabecular bone samples were measured with and without an interfering layer of overlying soft tissue. In addition, sound speed and attenuation in overlying adipose and lean tissues were measured separately. Uncorrected (without the soft tissue correction) ultrasound parameters for trabecular bone samples were determined as presented in Table 6.3. When applying numerical soft tissue correction, the ultrasound parameters were determined as presented in Table 6.4

Table 6.4: The mathematical definitions of soft tissue corrected ultrasound parameters (Study III).

Parameter	Equation
SOS	$\dfrac{c_l c_a c_w s_b}{c_l c_a (s_l + s_a + s_b) - (\Delta t c_w c_l c_a) - c_a c_w s_l - c_l c_w s_a}$
Attenuation*	$\frac{8.686}{s_b}(\ln(\frac{A_w(f)}{A_{lba}(f)}) + \ln((1 - R_{wl}(f))(1 - R_{lb}(f))(1 + R_{ab}(f))(1 + R_{wa}(f)))$ $-\alpha_l(f)s_l - \alpha_a(f)s_a)$
IRC	$\frac{8.686}{\Delta f}\int_{\Delta f}(\ln(\frac{A_n(f)}{A_r(f)}) - \ln(1 - R_{ws}^2(f)) + 2\alpha_s(f)s_s)$
AIB	$\frac{8.686}{\Delta f}\int_{\Delta f}(\ln(\frac{A_b(f)}{A_r(f)}) - \ln(1 - R_{ws}^2(f)) + 2\alpha_s(f)s_s)$
BUB	$\frac{8.686}{\Delta f}\int_{\Delta f}(\ln(\frac{A_b(f)}{A_r(f)}) + \frac{\alpha_b(f)c_b tw}{2} - \ln(1 - R_{ws}^2(f)) + 2\alpha_s(f)s_s)$

c = sound speed. Subscripts l, a, b and w refer to lean tissue, adipose tissue, bone and water, respectively. s = thickness of the sample. Δt = time of flight difference through the water bath with and without the soft tissue-bone combination, A_{lba} and A_w = ultrasound pressure amplitude spectra measured through the water bath with and without the soft tissue-bone combination, respectively. R = reflection coefficient. Subscripts wl, lb, ab, wa and ws refer to water-lean tissue, lean tissue-bone, adipose tissue-bone, water-adipose tissue and water-soft tissue interfaces, respectively. Δf = effective frequency range, A_n and A_r = ultrasound pressure amplitude spectra of the echo signal recorded from the sample surface and the reference, respectively. A_b = ultrasound pressure amplitude spectra recorded from the echo signal (backscattering part) from the inner structure of the sample. α = attenuation coefficient. Subscript s refers to soft tissue. tw = time window length for the determination of backscattering. *normalized Broadband Ultrasound Attenuation (nBUA) is determined as a slope of the linear part of the attenuation spectrum normalized with the sample thickness.

6.2.3 Dual frequency ultrasound technique

THEORY OF DUAL FREQUENCY ULTRASOUND TECHNIQUE

In Study IV, a new technique for the elimination of the soft tissue effect on bone ultrasound measurement was introduced. The DFUS technique utilizes prior knowledge of the values of the ultrasound (US) attenuation coefficient and speed at two frequencies in multilayered materials consisting of two different materials. The US reflection is measured from the front (first) and the back (last) surface of the multilayered structure using two different US frequencies. However, during *in vivo* measurement the US transducer is set against the skin and only the echo arising from the soft tissue-bone interface is recorded.

Ultrasound reflection amplitudes at low and high frequency (A_l, A_h) from the first surface of the object of interest (*e.g.* bone or elastomer 3 (figure 6.3)) can be expressed as follows:

$$A_l = H_l e^{-2\alpha_{1,l}x_1} e^{-2\alpha_{2,l}x_2} A_{0,l}, \tag{6.1}$$

$$A_h = H_h e^{-2\alpha_{1,h}x_1} e^{-2\alpha_{2,h}x_2} A_{0,h}, \tag{6.2}$$

where H is the term including ultrasound reflections at the surfaces of the interfering layers and the object of interest, α the attenuation coefficient and x the thickness
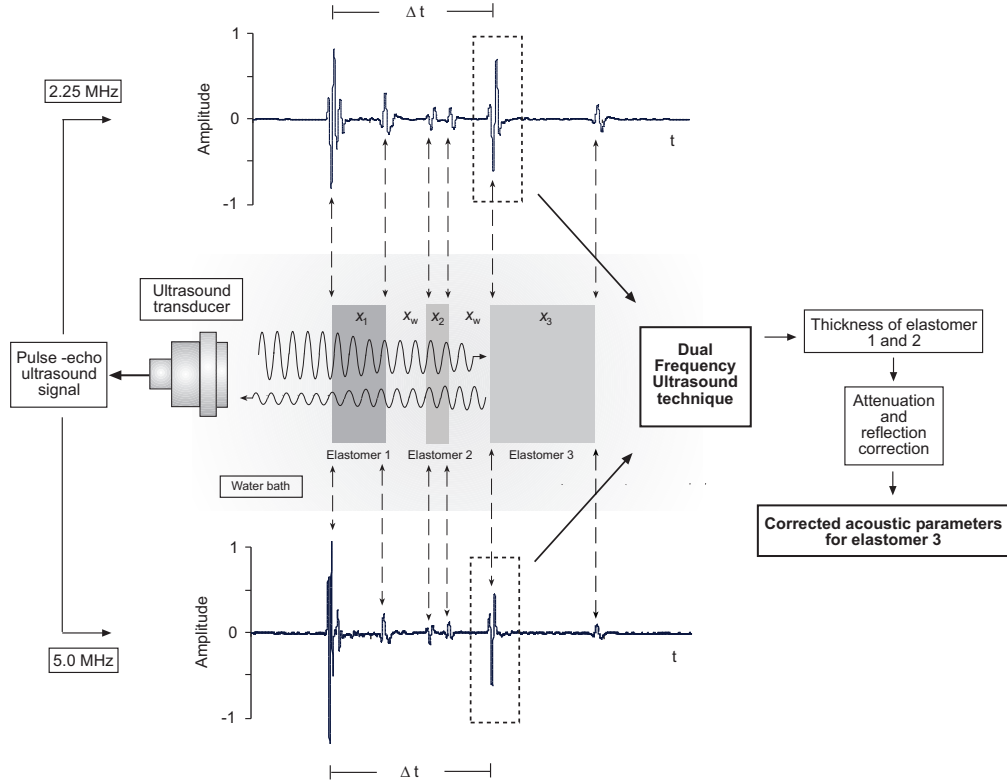
Figure 6.3: Experimental set-up for acoustic measurement of elastomer samples. The region of interest in the ultrasound signal is located at the echo arising from the surface of elastomer 3. The dual frequency ultrasound technique was used to minimize the artifacts induced by elastomers 1 and 2 in the determination of the acoustic properties of elastomer 3 (Study IV).

of an interfering layer. Subscripts 1 and 2 and l and h refer to interfering layers 1 and 2 and low and high ultrasound frequencies, respectively. $A_{0,l}$ and $A_{0,h}$ refer to ultrasound reflection amplitudes from the polished steel plate (reference) at low and high frequencies, respectively. If the ultrasound reflection coefficient depends on the frequency, it can be taken into account in the calculations:

$$H(f) = af^b, \tag{6.3}$$

where coefficients a and b denote the frequency dependence of the reflection term. Thus, the relation between the term H at low and high frequencies can be expressed as follows:

$$H_l = H_h(\frac{f_l}{f_h})^b = mH_h, \tag{6.4}$$

where f is the frequency and the coefficient m denotes the frequency dependence of H. The ultrasound reflection amplitude A_l (equation 6.1) can now be expressed as

follows:

$$A_l = m(\frac{A_h}{A_{0,h}}e^{2(\alpha_{1,h}x_1 + \alpha_{2,h}x_2)})e^{-2\alpha_{1,l}x_1}e^{-2\alpha_{2,l}x_2}A_{0,l}. \tag{6.5}$$

By substituting:

$$S = 2\alpha_{1,h} - 2\alpha_{1,l}, \tag{6.6}$$

$$J = 2\alpha_{2,h} - 2\alpha_{2,l}, \tag{6.7}$$

equation 6.5 can be expressed as follows:

$$\frac{A_l A_{0,h}}{m A_h A_{0,l}} = e^{x_1 S + x_2 J}. \tag{6.8}$$

The time difference Δt between the reflections from the first surface of the interfering layer and from the surface of the sample (see figure 6.3) can be written as follows:

$$\Delta t = 2(\frac{x_1}{c_1} + \frac{x_2}{c_2} + \frac{2x_w}{c_w}), \tag{6.9}$$

where c_1, c_2 and c_w are the average sound speeds measured at low and high ultrasound frequencies. The subscript w refers to water. The thickness of interfering layer 1 can be expressed as:

$$x_1 = (\frac{\Delta t}{2} - \frac{x_2}{c_2} - \frac{2x_w}{c_w})c_1. \tag{6.10}$$

The thickness of interfering layer 2 can now be solved from equations 6.8 and 6.10:

$$x_2 = \frac{\ln(\frac{1}{m}) + \ln(\frac{A_l}{A_{0,l}}) - \ln(\frac{A_h}{A_{0,h}}) - (\frac{\Delta t}{2} - \frac{2x_w}{c_w})c_1 S}{J - \frac{c_1 S}{c_2}}. \tag{6.11}$$

Using the determined thickness of layer 2, the thickness of interfering layer 1 can now be solved from equation 6.10.

DETERMINATION OF SOFT TISSUE COMPOSITION WITH THE DFUS TECHNIQUE

In measurement of a bone-soft tissue combination, the thickness of adipose (fat) and lean tissue can be solved with the dual frequency ultrasound technique. Reflection at the bone surface was found to be frequency independent (2.25 MHz vs. 5.0 MHz, Study III) and the reflections from the soft tissue surface and adipose-lean tissue interfaces were minimal, thus $b = 0$ (equation 6.3) and therefore $m = 1$ (equation 6.4). As there is no water layer ($x_w = 0$) between the adipose and lean tissue, equation 6.11 can be simplified and the lean tissue thickness can be expressed as:

$$x_2 = \frac{\ln(\frac{A_l}{A_{0,l}}) - \ln(\frac{A_h}{A_{0,h}}) - (\frac{\Delta t}{2})c_1 S}{J - \frac{c_1 S}{c_2}}, \tag{6.12}$$

where subscripts 1 and 2 refer to adipose and lean tissues, respectively.

NUMERICAL CORRECTION OF ULTRASOUND PARAMETERS

In Study IV, to eliminate the error induced by interfering elastomers, their thicknesses and acoustic properties must be known. The thicknesses of the interfering layers can be determined using the DFUS technique. In Study IV, three IRC values for each elastomer (3a, 3b and 3c) were determined: (1) IRC: parameter determined without the interfering overlying elastomers; (2) IRC_{uncorr}: parameter determined with the interfering overlying elastomers; and (3) IRC_{corr}: parameter determined with the interfering overlying elastomers by means of the DFUS attenuation correction. The corrected IRC (IRC_{corr}) can be determined as follows:

$$\text{IRC}_{corr} = \text{IRC}_{uncorr} + 2x_1\alpha_1 + 2x_2\alpha_2 + K_i, \tag{6.13}$$

where x is the elastomer thickness and α is the ultrasound attenuation coefficient for an investigated elastomer. Subscripts 1 and 2 refer to elastomers 1 and 2, respectively. K_i is the correction factor for the compensation of ultrasound reflections at the surfaces of elastomers 1 and 2:

$$K_i = 8.68 \ln((1 - R_1^2)^2 (1 - R_2^2)^2), \tag{6.14}$$

where R is the reflection coefficient. In addition, three average attenuation values for elastomers 3a-c were determined and named analogously with the IRC. The corrected average attenuation (AA_{corr}) can be determined as follows:

$$\text{AA}_{corr} = \text{AA}_{uncorr} - x_1\alpha_1 - x_2\alpha_2 - K_a, \tag{6.15}$$

where AA_{uncorr} is the uncorrected average attenuation and K_a is the correction factor for the compensation of ultrasound reflections at the surfaces of elastomers 1, 2 and 3.

$$K_a = 8.68 \ln((1 - R_1^2)^2 (1 - R_2^2)^2 (1 - R_3^2)). \tag{6.16}$$

To analyse precision errors, one elastomer (3c) was measured five times with and without the interfering overlying elastomers (combinations 1-3). Twenty measurements was conducted and the coefficient of variation (CV)(133) was determined.

For IRC and BUB measurements in living tissues, the soft tissue correction was conducted similarly as for elastomers (equation 6.13). Since no clear acoustic boundaries existed in the heterogeneous mixture of lean and adipose tissue, the K_i term could be neglected.

6.2.4 MicroCT measurement of trabecular bone

In Study II, the bone volume fraction (BV/TV, %), *i.e.* the volume fraction of the calcified matrix within the sample, was determined using a microCT (SkyScan 1072, SkyScan, Aartselaar, Belgium) (Hakulinen et al. 2006, (66)). The voxel size was 18 $\times$ 18 $\times$ 18 μm^3. Subsequently, the image data were segmented to include calcified matrix and marrow using the local threshold method (166).

6.2.5 Analyses of bone composition

DUAL ENERGY X-RAY MEASUREMENTS

In Studies I and III, the bone mineral densities (BMD, g/cm^2) of the samples were measured in a direction perpendicular to the parallel ends of the plugs using a Lunar Prodigy DXA system (GE Medical, Wessling, Germany) in the spine measurement mode (voltage = 76 kV, current = 0.75 mA). During measurement, the bone samples were placed in a water bath to simulate overlying soft tissues and to optimize the measurement accuracy. Volumetric BMD (vBMD, g/cm^3) values were calculated by normalizing measured areal BMD values with the sample thickness, as determined with a digital micrometer (Mitutoyo Co., Mexico City, Mexico).

WATER AND FAT CONTENT

In Study I, the volumes, weights and densities of the bone cylinders were determined using Archimedes' principle. Subsequently, the samples were freeze-dried (Christ Alpha 1-2, B. Braun Biotech International, Melsungen, Germany) for the determination of dry weights. To determine the fat-free weight of the sample, the fat was dissolved in acetone. The acetone was then removed from the samples by drying them at 45°C for 18 hours. Finally, the water and fat contents were determined by normalizing water and fat masses with the sample volume.

COMPOSITION OF CALCIFIED MATRIX

In Study I, the composition of calcified matrix (trabeculae) was determined by normalizing the biochemically determined collagen and proteoglycan masses and DXA-measured BMC with the calcified matrix volume, as determined with the microCT. To determine the masses of collagen and proteoglycan, the fat-free bone samples were pulverized. Some of the powder (approximately 20 mg) from each sample was taken for acid hydrolysis in 5 M hydrogen chloride (HCl) at 108°C for 16 hours, and hydroxyproline content was analyzed using a microplate assay (22). Collagen contains approximately 14% of hydroxyproline by mass, so estimates for total collagen contents were obtained by multiplying the hydroxyproline content by a factor of 7 (155). To investigate the yield of the assay, soluble rat type I collagen was also added to defatted bone samples before acid hydrolysis. The yield of the added collagen was $91.8 \pm 1.3\%$. Proteoglycans were extracted from the fat-free bone powder (approximately 20 mg) with 4 M guanidine hydrochloride (GuHCl) containing 0.2 M ethylenediamine tetraacetic acid (EDTA) in 50 mM sodium acetate buffer, pH 6.0, for 70 hours. Uronic acid content was then measured using a spectrophotometric assay (16). An estimate for proteoglycan content was derived by assuming that the major proteoglycans, decorin and biglycan (167), are present in approximately equal molar contents. The average molecular weight of glycosaminoglycan chains was assumed to be 30 kDa, based on decorin and biglycan molecular weights of 70 and 100 kDa, respectively (91, 146). Therefore, the uronic acid content represents approximately 26% of

the proteoglycan pool, which gives a factor of 3.78 to be used for the determination of proteoglycan content from the uronic acid results.

6.2.6 Analyses of bone mechanical properties

In Studies II and III, the mechanical properties of the bone samples were determined with servo-hydraulic material testing devices (Zwick 1484, Zwick GmbH & Co., KG, Ulm, Germany, and Instron 8874, Instron Co., Canton, MA, USA, respectively). During the test teflon foils were set between the sample surfaces and the compressive plates to minimize the friction between the surfaces (Study II). In Study II, bone samples were subjected to prestress of 0.25 MPa before testing, and preconditioned with five consecutive nondestructive cycles to 0.5% strain. Subsequently, the bone samples were destructively compressed to 5% strain, using the strain rate of 4.5×10^{-3} s^{-1}. In Study II, the measurement protocol was the same but the prestress applied was 0.10 MPa and the strain rate was 8.2×10^{-5} s^{-1}. In Study II, Young's modulus was determined as a linear fit to the stress-strain data between 45% and 60% of the maximum stress whereas in Study III Young's modulus was determined as a linear fit to the stress-strain data between 40% and 65% of the maximum stress. Ultimate strength was obtained as the maximum stress recorded during the test.

6.2.7 Numerical modelling

In Study I, Wave2000 Pro software (Cyberlogic Inc., New York, NY, USA) was used to simulate acoustic wave propagation through a trabecular bone sample. MicroCT images (one 2D cut of a 3D image set) of the trabecular samples (Study II) were used in the numerical modelling. The software solves the 2D wave equation by utilizing the finite difference time domain technique (FDTD). Earlier, we have demonstrated a good agreement between the experimental ultrasound measurements and two-dimensional (2D) numerical simulations (Hakulinen et al. 2006, (66)). The acoustic simulations were based on the real 2D microCT images of three trabecular bone samples with characteristic bone volume fraction ranging from 9% to 24%. Trabecular bone was assumed to consist of two components, *i.e.*, calcified tissue (trabeculae) and fat (marrow). The reference values of the acoustic and material properties for calcified matrix and fat were obtained from the material library of Wave2000 Pro. The reference value for the density of calcified matrix was set to be equal to that of the cortical bone (1850 kg/m^3). For fat tissue the density was set to 937 kg/m^3. In the model, calcified tissue was assumed to be an isotropic elastic solid with a Poisson ratio of 0.37 (5). In further simulations, trabecular architecture was kept constant while density and Young's modulus of the calcified matrix were altered. According to Bossy et al. (2004, Figure 6)(17) the bulk velocity of ultrasound in cortical bone increases by 140 m/s as the cortical bone density increases by 50 kg/m^3. Therefore, the values of Young's modulus were altered correspondingly, *i.e.* the increase in bulk velocity was 138-140 m/s when the calcified matrix density increased by 50 kg/m^3. These calculations were based on the relation between the ultrasound velocity and the material

properties of the isotropic elastic medium

$$c = \sqrt{\frac{E(1-\nu)}{\rho(1+\nu)(1-2\nu)}}, \qquad (6.17)$$

where c is the bulk velocity, E is the Young's modulus, ρ is the density and ν is Poisson's ratio. Similarly, for shear velocity (c_s) in isotropic elastic material

$$c_s = \sqrt{\frac{E}{2\rho(1+\nu)}}. \qquad (6.18)$$

The simulation geometry was identical to that of the experimental set-up. However, in the simulations the samples were immersed in deionized water (21°C) instead of PBS as in the experiments (Hakulinen et al. 2005, (67)). The characteristics of the 2.25 MHz ultrasound transducer used in the experimental measurements were adopted from the calibration data provided by the transducer manufacturer (Panametrics V304, Panametrics Inc., Waltham, MA, USA) and used in the simulations. The QUS parameters were determined from the simulation outputs similarly as from the experimentally measured signals.

In Study III, numerical simulations were conducted to investigate the effect of soft tissue thickness and composition on the measured attenuation and SOS values. The typical adipose to lean tissue ratio in human soft tissue, 25/75 (Morabia et al. 1999, (121)), was used to represent the real soft tissue composition in the simulations. The experimentally measured mean attenuation spectra and SOS values in bone and adipose and lean tissues were used for the simulations. Thereafter, the differences between uncorrected and corrected acoustic parameters were calculated with various soft tissue thickness and adipose to lean tissue ratios.

6.2.8 Statistical analyses

In Studies I - III, a normal distribution of compositional, mechanical and ultrasound parameters was tested with the Shapiro-Wilk test. Pearson's correlation analysis was used for the investigation of linear associations between the parameters. In Study I, to adjust the specific correlation analyses for other variables, partial correlation coefficients were calculated. In Study II, the Wilcoxon two-related-samples test was used to investigate the significance of the differences in ultrasound parameter values determined at discrete point at the ROI center and as a mean within the ROI. In addition, in Study II a stepwise linear regression analysis was used to investigate the relations between the ultimate strength and the linear combinations of ultrasound parameters. A p value of < 0.05 defined the statistical significance. SPSS v.11.5 and 14.0 softwares (SPSS Inc., Chicago, IL, USA) were used for the statistical analyses.

Results

7.1 Relations of acoustic, compositional and mechanical properties in trabecular bone

In Study I, QUS parameters were found to be significantly related to bone volume fraction ($r = 0.64$-0.84) and fat content ($r = -0.47$ - -0.54). In addition, linear correlations between the ultrasound parameters (SOS, nBUA, AA and AIB)) and the calcified matrix collagen content were statistically significant ($r = -0.46$ - -0.66, Table 7.1). Bone ultimate strength was significantly related to bone volume fraction ($r = 0.95$) and fat content ($r = -0.51$).

When the correlations were adjusted for other compositional variables (partial correlation), in addition to bone volume fraction, the collagen and proteoglycan content of calcified matrix were significant independent determinants of bone ultimate strength ($r = 0.63$ and $r = -0.55$, respectively, $p < 0.05$). Moreover, bone volume fraction was significantly related to SOS ($r = 0.68$). Only a moderate association was found between fat content and AIB ($r = -0.59$). Partial correlation analysis of ultrasound and composition parameters suggested that AIB and BUB are the only QUS parameters that are independent predictors of the calcified matrix collagen content ($r = -0.66$ *vs. r* $= -0.69$ and $r = -0.62$ *vs. r* $= -0.66$, respectively).

Table 7.1: Linear correlations between the mean values of ultrasound parameters within the circular ROI (88 mm^2) and the composition and ultimate strength of trabecular bone (n = 19 - 20). Partial correlation between parameters are shown in brackets.* $p < 0.05$, ** $p < 0.01$.

	BV/TV	Water content	Fat content	CC_{CM}	PC_{CM}	MC_{CM}	σ_{max}
SOS	0.84** (0.68**)	-0.18 (0.41)	-0.47* (0.08)	-0.59** (-0.46)	-0.14 (0.08)	-0.03 (-0.11)	0.75**
nBUA	0.64** (0.49)	0.08 (0.46)	-0.53* (0.07)	-0.46* (0.42)	0.07 (-0.11)	0.14 (0.23)	0.55*
AA	0.76** (0.29)	-0.13 (-0.01)	-0.54* (-0.39)	-0.54* (-0.50)	0.10 (0.15)	-0.10 (-0.35)	0.65**
IRC	0.84** (0.42)	-0.34 (-0.24)	-0.54* (-0.36)	-0.39 (-0.19)	-0.13 (-0.37)	0.13 (0.10)	0.89**
AIB	0.68** (-0.19)	-0.31 (-0.44)	-0.39 (-0.59*)	-0.66** (-0.69**)	-0.02 (0.10)	-0.08 (-0.26)	0.62**
BUB	0.80** (0.37)	-0.17 (-0.01)	-0.55* (-0.46)	-0.62** (-0.66**)	-0.06 (0.05)	-0.07 (-0.32)	0.70**
σ_{max}	0.95** (0.91**)	-0.42 (0.39)	-0.51* (0.40)	-0.31 (0.63*)	-0.02 (-0.55*)	0.21 (0.37)	-
vBMD	0.95** (0.99**)	-0.41 (-0.25)	-0.53* (-0.12)	-0.39 (-0.03)	0.12 (-0.24)	0.39 (0.98**)	0.92**

7.2 Spatial variation of ultrasound parameters

In Study II, SOS and AIB, but not nBUA, AA or IRC, were significantly different when determined as a mean value within the ROI or as a discrete value at the center of the ROI (p = 0.03, n = 19 - 20, Table 7.2). Linear correlation coefficients between the mean values of ultrasound parameters within the ROI and the ultimate strength were higher than those obtained for the single point measurements (Fig. 7.1). Based on the stepwise linear regression analysis, the linear combination of mean and SD of AA was a significantly stronger predictor of the ultimate strength than either the mean or SD of AA alone (r = 0.76 *vs.* 0.65 and -0.32, respectively). However, from variations (SD) of ultrasound parameters within the ROI, only SD of AIB was a significant predictor of ultimate strength (Fig. 7.1).

Table 7.2: Mean values of ultrasound parameters within the ROI and at the discrete measurement point of the ROI center. A significant difference was revealed in SOS and AIB (p = 0.03, n = 19 - 20), whereas no statistically significant differences were found in nBUA, AA or IRC.

	SOS (m/s)	nBUA (dB/MHz/cm)	AA (dB/cm)	IRC (dB)	AIB (2 μs tw) (dB)
ROI mean	2236	11.0	38.1	-12.7	-26.7
ROI Center	2451	10.3	39.3	-12.2	-27.8
ROI SD	359	3.3	4.1	2.6	3.3
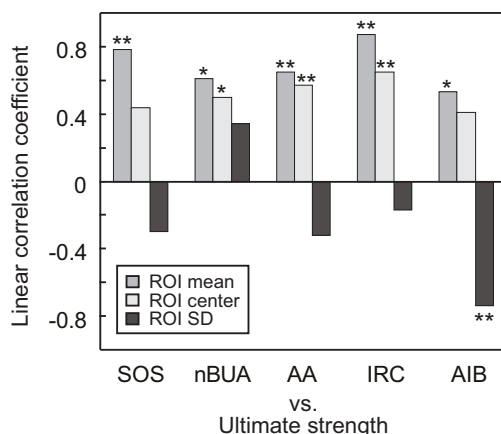
Figure 7.1: Linear correlations between the mean values of ultrasound parameters within the ROI and the ultimate strength showed a trend for higher values than those obtained for a single point measurement. SD of AIB within the ROI was a significant predictor of the ultimate strength (n = 19 - 20).   * $p < 0.05$, ** $p < 0.01$

7.3 Effect of time window length on AIB analysis

The increase in time window length increased the values of AIB within the ROI and decreased the variation of AIB within the ROI (Fig. 7.2). Further, the strength of cor-

relation between AIB and ultimate strength was dependent on the window length (Fig. 7.2). Mean AIB within the ROI predicted ultimate strength strongly only when assessed using a short time window (tw = 1 μs, r = 0.62). However, the strongest association (r = -0.82, p < 0.01) between SD of AIB within the ROI and ultimate strength was revealed with the long time window (tw = 4 μs).

Pulse-echo parameters (IRC and AIB) were analysed from the same echo signal and therefore these parameters were measured simultaneously. Based on the stepwise linear regression analysis, the linear combination of mean IRC and SD of AIB within the ROI served as a strong predictor (r = 0.92, p < 0.01) of the bone ultimate strength.
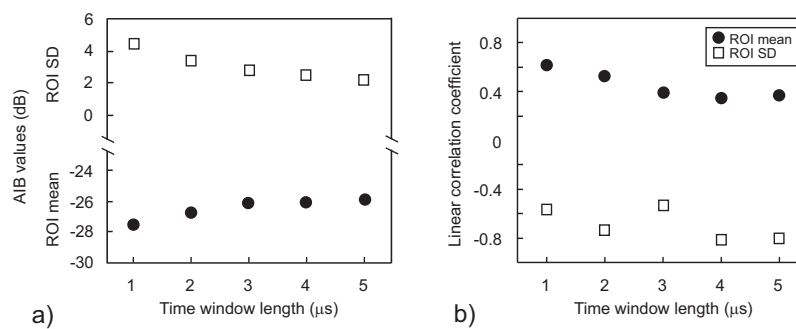

Figure 7.2: (a) The effect of time window length (tw) on the values and variation (SD) of AIB within the ROI. (b) Mean value of AIB within the ROI was significantly correlated with the ultimate strength only when using a short time window. SD of AIB within the ROI was significantly related with the ultimate strength (n = 19) also when determined by using long time windows. The time window length 1 μs corresponds to the distance of 1.1 mm when the mean SOS value for the bone samples (2236 m/s) is used.

7.4 Effect of overlying soft tissue on ultrasound measurement of trabecular bone

The overlying soft tissues induced significant errors in the measurement of bone acoustic properties (Fig. 7.3 and 7.4). The error in SOS (at the centre frequency of 5 MHz) was 7% when the effect of soft tissue was ignored (*i.e.* uncorrected values) and 3% when the soft tissue induced errors were mathematically minimized (*i.e.* corrected values) (Fig. 7.3). In Study III, all corrections were calculated using average SOS and attenuation values measured for adipose and lean tissue. At the centre frequency of 2.25 MHz, the error in average attenuation decreased from 22% to 3% (Fig. 7.3) and, in IRC, from 60% to 20%, when the soft tissue correction was applied (Fig. 7.4). Similarly, the error in BUB (at the centre frequency of 5 MHz) was reduced from 60% to 5% when the soft tissue induced errors were mathematically minimized (Fig. 7.4).
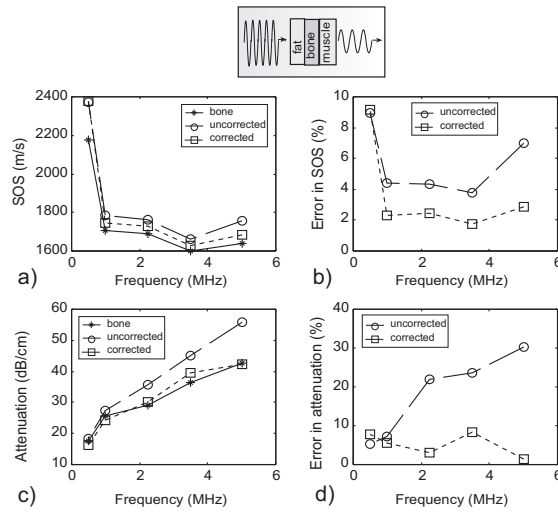
Figure 7.3: (a, c) The mean values of through-transmission parameters, SOS and average attenuation, before and after the numerical soft tissue correction and as measured without overlying soft tissues. (b, d) The error induced by soft tissue increased as a function of ultrasound frequency. The error could be effectively reduced by means of numerical correction (Study III).

Figure 7.4: (a, c) The mean values of pulse-echo parameters, IRC and BUB, before and after the soft tissue correction and as measured without the overlying soft tissues. (b, d) The error induced by soft tissue increased as a function of ultrasound frequency. The error could be effectively reduced by means of numerical correction (Study III).
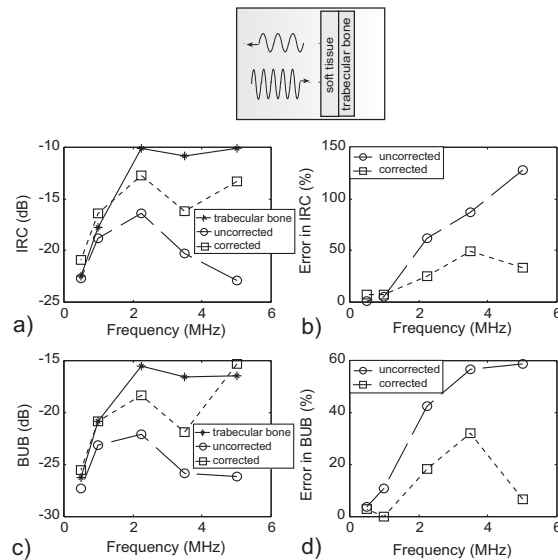
7.5 The dual frequency ultrasound technique

In Study IV, the relative precision (CV) of IRC and AA for the elastomers measured with 5.0 MHz were 1.2% and 1.3%, respectively, so only single measurements were conducted for other elastomer measurements. The DFUS technique reduced the mean error induced by interfering elastomers in IRC and in AA (at 2.25 MHz) from 37.5 - 77.5% to -12.0 - 4.9% and from 70.0 - 201.1% to -1.1 - 34.6%, respectively (Fig. 7.5). At the higher frequency (5.0 MHz), the DFUS technique reduced the mean error induced by interfering elastomers in IRC and in AA from 103.6 - 289.4% to -15.9 - 5.6% and from 33.8 - 158.3% to -29.7 - 6.5%, respectively (Fig. 7.5)

Figure 7.5: (a, b) The errors induced by interfering elastomers in IRC before and after the DFUS correction with a frequency of (a) 2.25 MHz and (b) 5.0 MHz. (c, d) The erro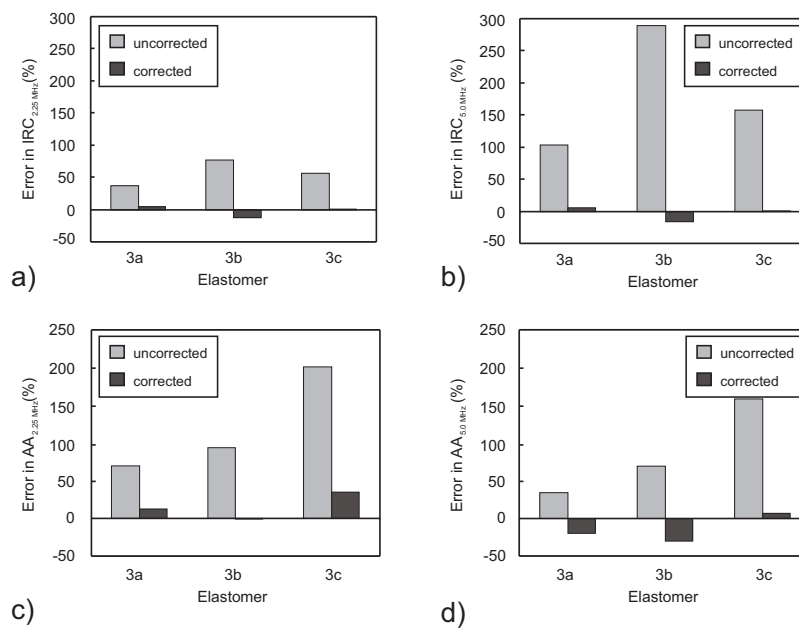rs induced by interfering elastomers in AA before and after the DFUS correction with a frequency of (c) 2.25 MHz and (d) 5.0 MHz. The absolute errors are determined by using the mean values of parameters (Table 7.3).

In the soft tissue-bone combination, the DFUS technique reduced the mean error in BUB and in IRC (at 5.0 MHz) from 58.6% to -4.9% and from 127.4% to 23.8%, respectively (Fig. 7.6).

Table 7.3: Values of the integrated reflection coefficient (IRC) and average attenuation (AA) of elastomers (3a-c) at 2.25 MHz and 5.0 MHz. The values of acoustic parameters for elastomers 3a-c were also determined with the interfering overlying elastomers (1 and 2) present (Fig. 6.3). Uncorrected (mean±SD) as well as corrected values (mean±SD, DFUS-technique) are also presented. The absolute errors are determined by using the mean values of parameters.

| | 2.25 MHz | | | 5.0 MHz | | |
	Elastomer 3a	Elastomer 3b	Elastomer 3c	Elastomer 3a	Elastomer 3b	Elastomer 3c
IRC (dB)	-35.7	-18.7	20.1	-31.7	-14.1	-19.3
AA (dB/cm)	10.5	17.1	6.1	30.0	42.8	17.8
Uncorrected values						
IRC (dB)	-49.0±2.7	-33.2±3.4	-31.4±1.7	-64.5±2.7	-55.0±5.5	-49.6±4.8
AA (dB/cm)	17.8±1.7	33.2±4.3	18.4±1.7	40.1±1.6	72.3±4.3	46.1±6.0
Corrected values						
IRC (dB)	-37.4±2.8	-16.5±2.8	-20.2±0.9	-33.4±2.8	-11.9±2.8	-19.4±0.9
AA (dB/cm)	11.8±1.7	16.9±4.5	8.2±0.6	24.0±1.9	30.1±4.5	19.0±1.9
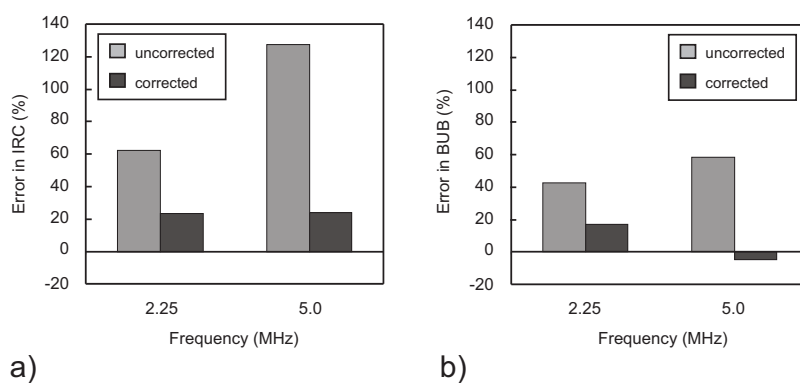
Figure 7.6: (a) The errors induced by overlying soft tissues in IRC before and after the DFUS correction at frequencies of 2.25 MHz and 5.0 MHz. (b) The errors induced by overlying soft tissues in BUB before and after the DFUS correction at frequencies of 2.25 MHz and 5.0 MHz. The absolute errors are determined by using the mean values of parameters (Table 7.4).

Table 7.4: Values (mean ± SD) of IRC and BUB in human trabecular bone at 2.25 MHz and 5.0 MHz. The acoustic properties of the bone samples were also determined with the overlying soft tissue layers. Uncorrected (mean±SD) as well as corrected values (mean±SD, DFUS-technique) are also presented. Absolute errors are calculated using the mean values of parameters.

| | Trabecular bone (n=26) | |
	2.25 MHz	5.0 MHz
IRC (dB)	-10.1±2.8	-10.1±3.1
BUB (dB)	-15.5±4.3	-16.5±3.8
Uncorrected values		
IRC (dB)	-16.4±4.0	-22.9±5.6
BUB (dB)	-22.1±4.8	-26.1±6.3
Corrected values		
IRC (dB)	-12.5±4.0	-12.5±4.0
BUB (dB)	-18.1±4.1	-15.7±4.8

Discussion

There are several challenges in the sensitive ultrasound diagnostics of trabecular bone. Clinical ultrasound devices are designed for the measurement of only peripheral sites. Novel ultrasound techniques should be developed for the measurement of central skeletal sites, and the selection of clinical reference measure is crucial in this endeavour. Most studies compare clinical ultrasound devices with DXA devices, the present gold standard in osteoporosis diagnosis. However, the DXA technique determines only the areal bone mineral density. Although it is an important determinant of bone strength, areal bone density is only one of many compositional, structural and geometrical factors affecting the probability of bone fracture. The potential of a novel ultrasound technique should be evaluated by comparing it with mechanical testing or the prevalence of fractures. Further, soft tissues overlying the bone are a major challenge in bone ultrasound measurements. Extensive individual variation in the thickness and composition of the soft tissue layer creates significant uncertainty. Moreover, the effect of the cortical layer has to be eliminated to obtain an accurate clinical ultrasound measurement of trabecular bone.

In the present thesis work, the composition of trabecular bone and calcified matrix was analysed and related to measured ultrasound parameters (Study I). Bone quantity was the strongest determinant of ultrasound parameters, while backscattering was also found to be significantly related to the collagen content of calcified matrix. In Study II, the diagnostic potential of a single point measurement and quantitative ultrasound imaging was compared. In addition, the spatial variation in ultrasound parameter values within the region of interest was investigated. A significant variation in ultrasound parameter values within the ROI was found, and the variation was found to be related to the mechanical parameters of trabecular bone. In Study III, the effect of overlying soft tissue on the ultrasound measurement of human trabecular bone was investigated at various frequencies. Soft tissue was found to induce significant errors in the ultrasound measurements of trabecular bone, and the effect of overlying soft tissue was found to increase with the ultrasound frequency. To minimize this source of measurement uncertainty, a new ultrasound method (DFUS) was introduced for soft tissue correction (Study IV). After DFUS correction, the error caused by the soft tissues on the QUS parameters was typically 1/10 of the error without any

correction.

EFFECT OF COMPOSITION ON THE ACOUSTIC AND MECHANICAL PROPERTIES OF TRA-
BECULAR BONE

In Study I, the partial correlation analysis indicated, as expected, that vBMD is af-
fected only by the bone volume fraction and mineral content of trabeculae. Inter-
estingly, partial correlation coefficients between the ultrasound parameters and bone
volume fraction were lower than the linear correlation coefficients. This suggests that
ultrasound parameters are influenced not only by bone volume fraction but also by
other compositional properties of bone. Furthermore, AIB showed a significant nega-
tive correlation, even after adjustment by other variables of composition, with the col-
lagen content of calcified matrix. Wear (1999)(169) has demonstrated less scattering
from elastic scatterers than from inelastic scatterers. Thus, the negative association
between AIB and collagen content may be explained by the variation in the elastic
properties of the scatter (78).

Since collagen is an important determinant of bone toughness, ultrasound backscat-
tering may provide information that is valuable when predicting fracture risk. Huo-
pio *et al.* (2004)(86) demonstrated that calcaneal ultrasound measurements predicted
early postmenopausal fractures as accurately as axial BMD. Fracture risk depends
on bone volume fraction, bone microstructure, and the composition and mechanical
properties of the calcified matrix as well as tissue turnover and microdamage accu-
mulation (25, 41). Bone ultimate strength and toughness are known to decrease sig-
nificantly along with collagen denaturation (168). In Study I, however, the ultimate
strength of trabecular bone was dependent on the bone volume fraction, but not on
the calcified matrix collagen content. Low variation (CV) in the calcified matrix col-
lagen content (11.2%) among the samples may explain this finding. Since there was
a considerable variation in donor age (24 - 76 years) and bone volume fraction (CV =
25.1%), the detected low variation in collagen content suggests that the collagen con-
tent of calcified matrix is relatively constant, exhibiting only minor variation within
the healthy population. However, quantitative information on bone organic compo-
sition, *e.g.* collagen content, could be of clinical benefit. Taken together, the present
findings suggest that acoustic measurements may provide diagnostically useful in-
formation not only about bone volume fraction but also about the composition of
trabecular calcified matrix.

SPATIAL VARIATION OF ULTRASOUND PARAMETERS

Variation of AIB within the ROI was found to be a significant predictor of bone ulti-
mate strength (Study II). Notably, the linear association between the variation of AIB
and ultimate strength was negative. Backscattering is related to scatterer size *i.e.* to
the thickness of the trabeculae or to the size of the pores (28). With small pore sizes,
e.g. in compact bone, trabecular bone is acoustically more homogenous diminishing
the variation of AIB. With greater pore sizes, *e.g.* in osteoporotic trabecular bone, tra-
becular bone is acoustically more heterogeneous, increasing the variation in AIB.

The high variation of ultrasound parameter values within the ROI raises the question of the value of point measurements and emphasizes the potential and role of parametric imaging. Since spatial variation in ultrasound parameters within *e.g.* the human proximal femur has been reported (138), the present findings are not surprising. The variation in acoustic properties may be explained by the structural characteristics of trabecular bone and the relatively small focus size of the applied transducer (a beam diameter (-6 dB) = 1.4 mm at focus). The more focused the beam is, the more it is affected by spatial variation in trabecular structure, density and mechanical properties. As the mean trabecular separation of the samples was between 0.3 and 0.8 mm, the variation in pore size and porosity can significantly contribute to the spatial variation detected in ultrasound parameter values. When conducting ultrasound imaging of trabecular bone, the phase cancellation effect (173) may also contribute to spatial variation in the backscattering parameters. Based on the investigations by Wear (173), the phase cancellation effects are more significant at high frequencies.

Effect of time window length on AIB analysis

In Study II, the association between AIB and ultimate strength was dependent on the length of the time window in ultrasound analysis. Mean AIB within the ROI predicted ultimate strength significantly only with a short time window ($r = 0.62$, tw = 1 μs), while significant associations were observed between the variation of AIB within the ROI and ultimate strength also when longer time windows were applied ($r = -0.82$, tw = 4 μs). Hoffmeister *et al.* (2002)(78) found weak negative and positive correlations ($r = -0.35 - 0.50$) between AIB and BMD in human trabecular bone *in vitro*. In bovine trabecular bone, Hoffmeister *et al.* (2000)(79) reported a weak negative association between AIB and apparent density ($r = -0.34 - -0.51$). Both studies (Hoffmeister *et al.* 2000, 2002) were conducted using an ultrasound transducer with a 2.25 MHz center frequency. In their analyses, a 4 μs time window length was applied. Recently, Hoffmeister *et al.* (2006)(77) reported a strong negative correlation ($r = -0.90$) between AIB and BMD, measured using a 5.0 MHz center frequency and a 4 μs time window length. The positive linear correlation between AIB and ultimate strength reported in Study II may be explained by the smaller effect of ultrasound attenuation. Since ultrasound backscattering arises from the deeper bone structures with long time windows, the backscattered sound is more attenuated. Further, ultrasound attenuation increases as a function of frequency, so the attenuation effect on AIB is higher at 5.0 MHz than at 2.25 MHz. This may explain the negative association between AIB and BMD reported by Hoffmeister *et al.* (2006) as well as the positive correlation between AIB and ultimate strength reported in Study II. In human trabecular bone, the true backscattering (broadband ultrasound backscattering, BUB), compensated by attenuation, is similar to that measured with 2.25 or 5.0 MHz (67). Our results suggest that the association between AIB and mechanical properties is positive when low frequencies and short time windows (in the present Study II, $f = 2.25$ MHz and tw = 1 μs) are used. Due to the attenuation, an increase in frequency and time window length diminishes the strength of the correlation between AIB and mechanical properties.

INVESTIGATION AND ELIMINATION OF THE EFFECT OF OVERLYING SOFT TISSUES ON QUS PARAMETERS

In Study III, overlying soft tissues were found to influence significantly the measured values of ultrasound attenuation, speed, reflection and backscattering in bone *in vitro*. The earlier studies have also demonstrated the influence of soft tissue on measured SOS in bone (29, 57, 99). Both Kotzki *et al.* (1994)(99) and Gomez *et al.* (1997)(57) reported that an increasing amount of adipose tissue significantly reduces the SOS values measured for bone. Similarly, ankle oedema has been shown to significantly decrease the measured BUA and SOS values (90). In Study III, the effect of soft tissues was eliminated by applying a numerical correction with a priori knowledge of soft tissue thickness and the lean and adipose tissue ratio. Soft tissue-related errors were seen to increase as a function of ultrasound frequency; however, with the numerical correction the soft tissue-induced errors could be effectively minimized.

In Study IV, a new dual frequency ultrasound (DFUS) method for soft tissue correction of bone ultrasound measurement was introduced. The initial validation with elastomer samples demonstrated a significant improvement in the accuracy of ultrasound measurements. The error of IRC at 5.0 MHz diminished from 103.6 - 289.4% to -15.9 - 5.6%. The reproducibility (CV) of the IRC measurements for the elastomers was 1.2% (at 5.0 MHz). Similarly, with human trabecular bone samples with 10 - 20 mm of overlying soft tissue the error in BUB (at 5.0 MHz) diminished from 58.6% to -4.9%.

Several patent descriptions (101, 103, 116, 120, 150, 184, 185) and scientific papers (111, 137) have been published on ultrasound techniques for the determination of soft tissue composition and the correction of the soft tissue effect in bone ultrasound measurements. However, these techniques are based on the through-transmission technique, assume a linear relation between attenuation and ultrasound frequency, or require detection of acoustic interfaces between the adipose and lean tissue layers.

In the patent GB2257253 (103), bone properties are measured with the through-transmission technique, while the effect of soft tissue is determined with the pulse-echo technique. The thickness of the soft tissue is analysed with the assumption of constant sound speed in the soft tissue. In addition, the reflections from the interfaces between the adipose and lean tissues must be detected in order to determine the thickness of the adipose and lean tissue layers.

In the patent US4512195 (120), a technique for the ultrasonic characterization of living body tissues is described. The thickness of the tissue layers is analysed from the echo signal by assuming constant sound speed in all tissues. Moreover, the ultrasound attenuation in tissues is analysed with the echo signals arising from the front and back surfaces of the tissue layers. With this technique, the front and back surfaces of the tissues have to be parallel in order to analyse the attenuation correction. Furthermore, all interfaces between the tissue layers must be acoustically visible.

Lu *et al.* (1995)(111) introduced a soft tissue correction method for backscatter measurements. In this technique, two different frequencies are used to estimate the effective attenuation coefficient of soft tissue between the ultrasound transducer and the

object of interest. However, this technique assumes constant sound speed in different tissues, so it estimates the thickness of tissues differently than the DFUS technique. In addition, the technique assumes a linear relation between the attenuation of ultrasound in soft tissue and frequency. The DFUS technique is free from this assumption.

In summary, the DFUS technique introduced in Study IV is the first pulse-echo ultrasound technique capable of determining the amount and composition of overlying soft tissue without reflection information from the interfaces between adipose and lean tissues, and may therefore enhance the accuracy of clinical ultrasound measurements significantly.

Summary and conclusions

The gold standard in osteoporosis diagnosis is currently dual energy X-ray absorptiometry. DXA provides information about the areal bone mineral density. However, bone strength depends on both the quantity and quality of the calcified matrix of trabecular bone. These are the properties which also affect the QUS measurements. Unfortunately, current clinical QUS measurements are only moderately good predictors of osteoporotic bone fractures.

In this thesis work, the effect of trabecular bone composition on ultrasound, DXA and mechanical parameters was analysed. The effect of spatial variation in 2D ultrasound parametric images was also investigated, as was the effect of overlying soft tissue on trabecular bone ultrasound measurements. A novel soft tissue correction method (DFUS) was introduced and evaluated.

The most important results can be summarized as follows:

1. Ultrasound backscattering is a significant predictor of collagen content in calcified matrix.

2. Spatial variation of ultrasound backscattering is significantly associated with the ultimate strength of trabecular bone.

3. Overlying soft tissues can induce significant errors in the values of ultrasound parameters of trabecular bone.

4. The DFUS technique can be used to determine the thickness and composition of overlying soft tissues. Therefore, the DFUS technique reduces significantly the error induced by soft tissues in the ultrasound measurement of bone.

1. J. Aerssens, S. Boonen, J. Joly, and J. Dequeker. Variations in trabecular bone composition with anatomical site and age: potential implications for bone quality assessment. *J Endocrinol*, 155(3):411–421, 1997.

2. P. Alexandersen, F. de Terlizzi, L. B. Tanko, Y. Z. Bagger, and C. Christiansen. Comparison of quantitative ultrasound of the phalanges with conventional bone densitometry in healthy postmenopausal women. *Osteoporos Int*, 16(9):1071–1078, 2005.

3. J. M. Alves, J. T. Ryaby, J. J. Kaufman, F. P. Magee, and R. S. Siffert. Influence of marrow on ultrasonic velocity and attenuation in bovine trabecular bone. *Calcif Tissue Int*, 58:362–367, 1996.

4. R. B. Ashman, J. D. Corin, and C. H. Turner. Elastic properties of cancellous bone: measurement by an ultrasonic technique. *J Biomech*, 20(10):979–986, 1987.

5. R. B. Ashman, S. C. Cowin, W. C. Van Buskirk, and J. C. Rice. A continuous wave technique for the measurement of the elastic properties of cortical bone. *J Biomech*, 17(5):349–361, 1984.

6. X. Banse, J. Devogelaer, A. Lafosse, T. J. Sims, M. Grynpas, and A. J. Bailey. Cross-link profile of bone collagen correlates with structural organization of trabeculae. *Bone*, 31(1):70–76, 2002.

7. M. Barger-Lux and R. Recker. Bone microstructure in osteoporosis: transilial biopsy and histomorphometry. *Top Magn Reson Imaging*, 13(5):297–305, 2002.

8. R. Barkmann, E. Kantorovich, C. Singal, D. Hans, H. K. Genant, M. Heller, and C. C. Gluer. A new method for quantitative ultrasound measurements at multiple skeletal sites: first results of precision and fracture discrimination. *J Clin Densitom*, 3(1):1–7, 2000.

9. R. Barkmann, P. Laugier, U. Moser, S. Dencks, M. Klausner, F. Padilla, G. Haiat, M. Heller, and C. C. Gluer. In vivo measurements of ultrasound transmission through the human proximal femur. *Ultrasound Med Biol*, 34(7):1186–1190, 2008.

10. R. Barkmann, P. Laugier, U. Moser, S. Dencks, F. Padilla, G. Haiat, M. Heller, and C. C. Gluer. A method for the estimation of femoral bone mineral density from variables of ultrasound transmission through the human femur. *Bone*, 40(1):37–44, 2007.

11. J. C. Behrens, P. S. Walker, and H. Shoji. Variations in strength and structure of cancellous bone at the knee. *J Biomech*, 7(3):201–207, 1974.

12. M. A. Biot. Theory of propagation of elastic waves in a fluid saturated porous solid i. low frequency range. *J Acoust Soc Am*, 28:168–178, 1956.

13. M. A. Biot. Theory of propagation of elastic waves in a fluid saturated porous solid II. higher frequency range. *J Acoust Soc Am*, 28(2):179–191, 1956.

14. D. Blackstock. *Fundamentals of physical acoustics*. John Wiley and Sons, New York, 1 edition, 2000.

15. W. Bloom and D. Fawcett. *A textbook of histology*. W.B. Saunders Company, Philadelphia, 9 edition, 1968.

16. N. Blumenkrantz and G. Asboe-Hansen. New method for quantitative determination of uronic acids. *Anal Biochem*, 54(2):484–489, 1973.

17. E. Bossy, M. Talmant, F. Peyrin, L. Akrout, P. Cloetents, and P. Laugier. An in vitro study of the ultrasonic axial transmission technique at the radius: 1-MHz velocity measurements are sensitive to both mineralization and intracortical porosity. *J Bone Miner Res*, 19(9):1548–1556, 2004.

18. S. Boutroy, M. Bouxsein, F. Munoz, and P. D. Delmas. In vivo assessment of trabecular bone microarchitecture by high-resolution peripheral quantitative computed tomography. *J Clin Endocrinol Metab*, 90(12):6508–6515, 2005.

19. M. L. Bouxsein, L. Palermo, C. Yeung, and D. M. Black. Digital X-ray radiogrammetry predicts hip, wrist and vertebral fracture risk in elderly women: a prospective analysis from the study of osteoporotic fractures. *Osteoporos Int*, 13(5):358–365, 2002.

20. M. Boyanov, A. Shinkov, and R. Nestorova. Bone density measurement: quantitative ultrasound of the calcaneus and distal radius. A comparison with dual spectrum X-ray absorptiometry. *Dtsch Med Wochenschr*, 132(16):869–873, 2007.

21. K. Brear, J. D. Currey, S. Raines, and K. J. Smith. Density and temperature effects on some mechanical properties of cancellous bone. *Eng Med*, 17(4):163–167, 1988.

22. S. Brown, M. Worsfold, and C. Sharp. Microplate assay for the measurement of hydroxyproline in acid-hydrolyzed tissue samples. *Biotechniques*, 30:38–42, 2001.

23. T. A. Burgers, J. Mason, G. Niebur, and H. L. Ploeg. Compressive properties of trabecular bone in the distal femur. *J Biomech*, 41(5):1077–1085, 2008.

24. D. Burr. The contribution of the organic matrix to bone's material properties. *Bone*, 31(1):8–11, 2002.

25. D. Burr. Bone quality: Understanding what matters. *J Musculoskel Neuronal Interact*, 4(2):184–186, 2004.

26. D. Carter, G. Schwab, and D. Spengler. Tensile fracture of cancellous bone. *Acta Orthop Scand*, 51(5):733–741, 1980.

27. D. R. Carter and W. C. Hayes. The compressive behavior of bone as a two-phase porous structure. *J Bone Joint Surg Am*, 59(7):954–962, 1977.

28. S. Chaffai, F. Peyrin, S. Nuzzo, R. Porcher, G. Berger, and P. Laugier. Ultrasonic characterization of human cancellous bone using transmission and backscatter measurements: Relationship to density and microstructure. *Bone*, 30(1):229–236, 2002.

29. C. Chappard, E. Camus, F. Lefebvre, G. Guillot, J. Bittoun, G. Berger, and P. Laugier. Evaluation of error bounds on calcaneal speed of sound caused by surrounding soft tissue. *J Clin Densitom*, 3(2):121–131, 2000.

30. S. Cheng, C. F. Njeh, B. Fan, X. Cheng, D. Hans, L. Wang, T. Fuerst, and H. K. Genant. Influence of region of interest and bone size on calcaneal BMD: implications for the accuracy of quantitative ultrasound assessments at the calcaneus. *Br J Radiol*, 75(889):59–68, 2002.

31. S. Cheng, F. A. Tylavsky, E. S. Orwoll, J. Y. Rho, and L. D. Carbone. The role of collagen abnormalities in ultrasound and densitometry assessment: In vivo evidence. *Calcif Tissue Int*, 64(6):470–476, 1999.

32. E. Cherin, A. Saied, P. Laugier, P. Netter, and G. Berger. Evaluation of acoustical parameter sensitivity to age-related and osteoarthritic changes in articular cartilage using 50-MHz ultrasound. *Ultrasound Med Biol*, 24(3):341–354., 1998.

33. Y. Chevalier, D. Pahr, H. Allmer, M. Charlebois, and P. Zysset. Validation of a voxel-based FE method for prediction of the uniaxial apparent modulus of human trabecular bone using macroscopic mechanical tests and nanoindentation. *J Biomech*, 40:3333–3340, 2007.

34. M. J. Ciarelli, S. A. Goldstein, J. L. Kuhn, D. D. Cody, and M. B. Brown. Evaluation of orthogonal mechanical properties and density of human trabecular bone from the major metaphyseal regions with materials testing and computed tomography. *J Orthop Res*, 9(5):674–682, 1991.

35. J. A. Clowes, R. Eastell, and N. F. Peel. The discriminative ability of peripheral and axial bone measurements to identify proximal femoral, vertebral, distal forearm and proximal humeral fractures: a case control study. *Osteoporos Int*, 16(12):1794–1802, 2005.

36. A. Cranney, S. A. Jamal, J. F. Tsang, R. G. Josse, and W. D. Leslie. Low bone mineral density and fracture burden in postmenopausal women. *CMAJ*, 177(6):575–580, 2007.

37. J. Damilakis, A. Papadakis, K. Perisinakis, and N. Gourtsoyiannis. Broadband ultrasound attenuation imaging: influence of location of region of measurement. *Eur Radiol*, 11:1117–1122, 2001.

38. S. Dencks, R. Barkmann, F. Padilla, G. Haiat, P. Laugier, and C. C. Gluer. Wavelet-based signal processing of in vitro ultrasonic measurements at the proximal femur. *Ultrasound Med Biol*, 33(6):970–980, 2007.

39. E. Diessel, T. Fuerst, C. F. Njeh, D. Hans, S. Cheng, and H. K. Genant. Comparison of an imaging heel quantitative ultrasound device (DTU-one) with densitometric and ultrasonic measurements. *Br J Radiol*, 73(865):23–30, 2000.

40. M. Ding, M. Dalstra, C. C. Danielsen, J. Kabel, I. Hvid, and F. Linde. Age variations in the properties of human tibial trabecular bone. *J Bone Joint Surg Br*, 79(6):995–1002, 1997.

41. L. J. Dominguez, M. Barbagallo, and L. Moro. Collagen overglycosylation: A biochemical feature that may contribute to bone quality. *Biochem Biophys Res Commun*, 330:1–4, 2005.

42. I. A. Dontas and C. K. Yiannakopoulos. Risk factors and prevention of osteoporosis-related fractures. *J Musculoskelet Neuronal Interact*, 7(3):268–272, 2007.

43. F. A. Duck, A. C. Baker, and H. C. Starritt. *Ultrasound in medicine*. Medical Science Series. Institute of Physics Publishing, London, 1998.

44. F. Eckstein, M. Matsuura, V. Kuhn, M. Priemel, R. Muller, T. Link, and E. Lochmuller. Sex differences of human trabecular bone microstructure in aging are site dependent. *J Bone Miner Res*, 22(6):817–824, 2007.

45. J. Faran. Sound scattering by solid cylinders and spheres. *J Acoust Soc Am*, 23(4):405–418, 1951.

46. Z. E. Fellah, J. Y. Chapelon, S. Berger, W. Lauriks, and C. Depollier. Ultrasonic wave propagation in human cancellous bone: application of Biot theory. *J Acoust Soc Am*, 116(1):61–73, 2004.

47. B. Fournier, C. Chappard, C. Roux, G. Berger, and P. Laugier. Quantitative ultrasound imaging at the calcaneus using an automatic region of interest. *Osteoporos Int*, 7(4):363–369, 1997.

48. P. Fratzl, H. Gupta, E. Paschalis, and P. Roschger. Structure and mechanical quality of the collagen-mineral nano-composite in bone. *J Mater Chem*, 14:2115–2123, 2004.

49. M. L. Frost, G. M. Blake, and I. Fogelman. Does quantitative ultrasound imaging enhance precision and discrimination? *Osteoporos Int*, 11:425–433, 2000.

50. M. L. Frost, G. M. Blake, and I. Fogelman. Quantitative ultrasound and bone mineral density are equally strongly associated with risk factors for osteoporosis. *J Bone Miner Res*, 16(2):406–416., 2001.

51. J. Galante, W. Rostoker, and R. D. Ray. Physical properties of trabecular bone. *Calcif Tissue Res*, 5(3):236–246, 1970.

52. L. Gartner and J. Hiatt. *Color textbook of histology*. W.B. Saunders Company, Philadelphia, 2 edition, 2001.

53. C. C. Glüer. Quantitative ultrasound techniques for the assessment of osteoporosis: expert agreement on current status. The International Quantitative Ultrasound Consensus Group. *J Bone Miner Res*, 12(8):1280–1288, 1997.

54. C.-C. Glüer, R. Eastell, D. M. Reid, D. Felsenberg, C. Roux, R. Barkmann, W. Timm, T. Blenk, G. Armbrecht, A. Stewart, J. Clowes, F. E. Thomasius, and S. Kolta. Association of five quantitative ultrasound devices and bone densitometry with osteoporotic vertebral fractures in a population-based sample: the OPUS stydy. *J Bone Miner Res*, 19(5):782–793, 2004.

55. C. C. Glüer, C. Y. Wu, M. Jergas, S. A. Goldstein, and H. K. Genant. Three quantitative ultrasound parameters reflect bone structure. *Calcif Tissue Int*, 55(1):46–52, 1994.

56. S. A. Goldstein, D. L. Wilson, D. A. Sonstegard, and L. S. Matthews. The mechanical properties of human tibial trabecular bone as a function of metaphyseal location. *J Biomech*, 16(12):965–969, 1983.

57. M. Gomez, F. Aguado, J. Manuel, J. M. Menendez, M. Revilla, L. F. Villa, J. Cortes, and H. Rico. Influence of soft tissue (fat and fat-free mass) on ultrasound bone velocity: an in vivo study. *Invest Radiol*, 32(10):609–612, 1997.

58. H. Gong, M. Zhang, H. Yeung, and L. Qin. Regional variations in microstructural properties of vertebral trabeculae with aging. *J Bone Miner Metab*, 23:174–180, 2005.

59. O. Gurevitch, S. Slavin, and A. Feldman. Conversion of red marrow into yellow - cause and mechanism. *Med Hypotheses*, 69:531–536, 2007.

60. G. Haiat, F. Padilla, R. Barkmann, S. Dencks, U. Moser, C. C. Gluer, and P. Laugier. Optimal prediction of bone mineral density with ultrasonic measurements in excised human femur. *Calcif Tissue Int*, 77(3):186–192, 2005.

61. G. Haiat, F. Padilla, R. Barkmann, C. C. Gluer, and P. Laugier. Numerical simulation of the dependence of quantitative ultrasonic parameters on trabecular bone microarchitecture and elastic constants. *Ultrasonics*, 44 Suppl 1:e289–294, 2006.

62. G. Haiat, F. Padilla, R. Barkmann, S. Kolta, C. Latremouille, C. C. Gluer, and P. Laugier. In vitro speed of sound measurement at intact human femur specimens. *Ultrasound Med Biol*, 31(7):987–996, 2005.

63. G. Haiat, F. Padilla, R. O. Cleveland, and P. Laugier. Effects of frequency-dependent attenuation and velocity dispersion on in vitro ultrasound velocity measurements in intact human femur specimens. *IEEE Trans Ultrason Ferroelectr Freq Control*, 53(1):39–51, 2006.

64. G. Haiat, F. Padilla, F. Peyrin, and P. Laugier. Variation of ultrasonic parameters with microstructure and material properties of trabecular bone: a 3D model simulation. *J Bone Miner Res*, 22(5):665–674, 2007.

65. T. J. Haire and C. M. Langton. Biot theory: a review of its application to ultrasound propagation through cancellous bone. *Bone*, 24(4):291–295, 1999.

66. M. Hakulinen, J. Day, J. Töyräs, H. Weinans, and J. Jurvelin. Ultrasonic characterization of human trabecular bone microstructure. *Phys Med Biol*, 51(6):1633–1648, 2006.

67. M. A. Hakulinen, J. S. Day, J. Töyräs, M. Timonen, H. Kröger, H. Weinans, I. Kiviranta, and J. S. Jurvelin. Prediction of density and mechanical properties of human trabecular bone in vitro by using ultrasound transmission and backscattering measurements at 0.2-6.7 MHz frequency range. *Phys Med Biol*, 50:1–14, 2005.

68. M. A. Hakulinen, J. Töyräs, S. Saarakkala, J. Hirvonen, H. Kröger, and J. S. Jurvelin. Ability of ultrasound backscattering to predict mechanical properties of bovine trabecular bone. *Ultrasound Med Biol*, 30(7):919–927, 2004.

69. M. Halawa, A. Lee, R. Ling, and S. Vangala. The shear strength of trabecular bone from the femur, and some factors affecting the shear strength of the cement-bone interface. *Arch Orthop Traumat Surg*, 92:19–30, 1978.

70. D. Hans, P. Dargent-Molina, A. M. Schott, J. L. Sebert, C. Cormier, P. O. Kotzki, P. D. Delmas, J. M. Pouilles, G. Breart, and P. J. Meunier. Ultrasonographic heel measurements to predict hip fracture in elderly women: the EPIDOS prospective study. *Lancet*, 348:511–514, 1996.

71. C. T. Hasselman, M. T. Vogt, K. L. Stone, J. A. Cauley, and S. F. Conti. Foot and ankle fractures in elderly white woman. Incidence and risk factors. *J Bone Joint Surg Am*, 85(5):820–824, 2003.

72. T. Hildebrand, A. Laib, R. Muller, J. Dequeker, and P. Ruegsegger. Direct three-dimensional morphometric analysis of human cancellous bone: Microstructural data from spine, femur, iliac crest, and calcaneus. *J Bone Miner Res*, 14(7):1167–1174, 1999.

73. T. Hildebrand and P. Ruegsegger. A new method for the model-independent assessment of thickness in three-dimensional images. *J Microsc*, 185(1):67–75, 1996.

74. T. Hildebrand and P. Ruegsegger. Quantification of bone microarchitecture with the structure model index. *Comput Methods Biomech Biomed Engin*, 1(1):15–23, 1997.

75. C. Hill, J. Bamber, and G. ter Haar. *Physical principles of medical ultrasonics*. John Wiley and Sons, West Sussex, 2 edition, 2004.

76. B. K. Hoffmeister, J. A. Auwarter, and J. Y. Rho. Effect of marrow on the high frequency ultrasonic properties of cancellous bone. *Phys Med Biol*, 47:3419–3427, 2002.

77. B. K. Hoffmeister, r. Jones, C. I., G. J. Caldwell, and S. C. Kaste. Ultrasonic characterization of cancellous bone using apparent integrated backscatter. *Phys Med Biol*, 51(11):2715–2727, 2006.

78. B. K. Hoffmeister, S. A. Whitten, S. C. Kaste, and J. Y. Rho. Effect of collagen and mineral content on the high-frequency ultrasonic properties of human cancellous bone. *Osteoporos Int*, 13(1):26–32., 2002.

79. B. K. Hoffmeister, S. A. Whitten, and J. Y. Rho. Low-megahertz ultrasonic properties of bovine cancellous bone. *Bone*, 26(6):635–642., 2000.

80. J. Homminga, B. Van-Rietbergen, E. Lochmuller, H. Weinans, F. Eckstein, and R. Huiskes. The osteoporotic vertebral structure is well adapted to the loads of daily life, but not to infrequent "error" loads. *Bone*, 34:510–516, 2004.

81. A. Hosokawa. Simulation of ultrasound propagation through bovine cancellous bone using elastic and Biot's finite-difference time-domain methods. *J Acoust Soc Am*, 118(3 Pt 1):1782–1789, 2005.

82. A. Hosokawa. Ultrasonic pulse waves in cancellous bone analyzed by finite-difference time-domain methods. *Ultrasonics*, 44 Suppl 1:e227–231, 2006.

83. A. Hosokawa and T. Otani. Ultrasonic wave propagation in bovine cancellous bone. *J Acoust Soc Am*, 101(1):558–562, 1997.

84. E. R. Hughes, T. G. Leighton, G. W. Petley, and P. R. White. Ultrasonic propagation in cancellous bone: a new stratified model. *Ultrasound Med Biol*, 25(5):811–821, 1999.

85. E. R. Hughes, T. G. Leighton, P. R. White, and G. W. Petley. Investigation of an anisotropic tortuosity in a biot model of ultrasonic propagation in cancellous bone. *J Acoust Soc Am*, 121(1):568–574, 2007.

86. J. Huopio, H. Kröger, R. Honkanen, J. S. Jurvelin, S. Saarikoski, and E. Alhava. Calcaneal ultrasound predicts early postmenopausal fractures as well as axial BMD. a prospective study of 422 woman. *Osteoporos Int*, 15(3):190–195, 2004.

87. I. Hvid and S. L. Hansen. Trabecular bone strength patterns at the proximal tibial epiphysis. *J Orthop Res*, 3(4):464–472, 1985.

88. B. M. Ingle, K. E. Sherwood, and R. Eastell. Comparison of two methods for measuring ultrasound properties of the heel in postmenopausal woman. *Osteoporos Int*, 12:500–505, 2001.

89. F. Jenson, F. Padilla, and P. Laugier. Prediction of frequency-dependent ultrasonic backscatter in cancellous bone using statistical weak scattering model. *Ultrasound Med Biol*, 29(3):455–464, 2003.

90. A. Johansen and M. D. Stone. The effect of ankle oedema on bone ultrasound assessment at the heel. *Osteoporos Int*, 7(1):44–47, 1997.

91. B. Johnstone, M. Markopoulos, P. Neame, and B. Caterson. Identification and characterization of glycanated and non-glycanated forms of biglycan and decorin in the human intervertebral disc. *Biochem J*, 292(3):661–666, 1993.

92. H. Jongen, J. Thijssen, M. van den Aarssen, and W. Verhoef. A general model for the absorption of ultrasound by biological tissues and experimental verification. *J Acoust Soc Am*, 79(2):535–540, 1986.

93. H. L. Jorgensen and C. Hassager. Improved reproducibility of broadband ultrasound attenuation of the os calcis by using a specific region of interest. *Bone*, 21(1):109–112, 1997.

94. L. Junqueira, J. Carneiro, and R. Kelley. *Basic histology*. Appleton and Lange, 7 edition, 1992.

95. J. Kanis. Diagnosis of osteoporosis and assessment of fracture risk. *Lancet*, 360:1929–1936, 2002.

96. J. A. Kanis, E. V. McCloskey, H. Johansson, A. Oden, r. Melton, L. J., and N. Khaltaev. A reference standard for the description of osteoporosis. *Bone*, 42(3):467–475, 2008.

97. J. A. Kanis, A. Oden, O. Johnell, H. Johansson, C. De Laet, J. Brown, P. Burckhardt, C. Cooper, C. Christiansen, S. Cummings, J. A. Eisman, S. Fujiwara, C. Gluer, D. Goltzman, D. Hans, M. A. Krieg, A. La Croix, E. McCloskey, D. Mellstrom, r. Melton, L. J., H. Pols, J. Reeve, K. Sanders, A. M. Schott, A. Silman, D. Torgerson, T. van Staa, N. B. Watts, and N. Yoshimura. The use of clinical risk factors enhances the performance of BMD in the prediction of hip and osteoporotic fractures in men and women. *Osteoporos Int*, 18(8):1033–1046, 2007.

98. J. Karjalainen, O. Riekkinen, J. Töyräs, H. Kröger, and J. S. Jurvelin. Ultrasonic assessment of cortical bone thickness in vitro and in vivo. *IEEE Trans Ultrason Ferroelectr Freq Control*, 55(10):2191–2197, 2008.

99. P. O. Kotzki, D. Buyck, D. Hans, E. Thomas, F. Bonnel, F. Favier, P. J. Meunier, and M. Rossi. Influence of fat on ultrasound measurements of the os calcis. *Calcif Tissue Int*, 54(2):91–95, 1994.

100. Y. Lai, L. Qin, H. Yeung, K. Lee, and K. Chan. Regional differences in trabecular BMD and micro-architecture of weight-bearing bone under habitual gait loading - A pQCT and microCT study in human cadavers. *Bone*, 37:274–282, 2005.

101. P. Lang, S. Grampp, and J. Mendlein. Measurement of body fat using ultrasound methods and devices. *United States Patent*, 5,941,825, 1999.

102. S. B. Lang. Ultrasonic method for measuring elastic coefficients of bone and results on fresh and dried bovine bones. *IEEE Trans Biomed Eng*, 17(2):101–105, 1970.

103. C. M. Langton. Ultrasound bone analyser. *UK Patent Application*, 2,257,253A, 1993.

104. C. M. Langton, S. B. Palmer, and R. W. Porter. The measurement of broadband ultrasonic attenuation in cancellous bone. *Eng Med*, 13(2):89–91, 1984.

105. K. I. Lee, E. R. Hughes, V. F. Humphrey, T. G. Leighton, and M. J. Choi. Empirical angle-dependent Biot and MBA models for acoustic anisotropy in cancellous bone. *Phys Med Biol*, 52(1):59–73, 2007.

106. W. Lin, Y. X. Qin, and C. Rubin. Ultrasonic wave propagation in trabecular bone predicted by the stratified model. *Ann Biomed Eng*, 29(9):781–790, 2001.

107. O. Lindahl. Mechanical properties of dried defatted spongy bone. *Acta Orthop Scand*, 47(1):11–19, 1976.

108. F. Linde. Elastic and viscoelastic properties of trabecular bone by a compression testing approach. *Dan Med Bull*, 41(2):119–138, 1994.

109. F. Linde and I. Hvid. Stiffness behaviour of trabecular bone specimens. *J Biomech*, 20(1):83–89, 1987.

110. F. Linde and H. C. Sorensen. The effect of different storage methods on the mechanical properties of trabecular bone. *J Biomech*, 26(10):1249–1252, 1993.

111. Z. F. Lu, J. A. Zagzebski, E. L. Madsen, and F. Dong. A method for estimating an overlying layer correction in quantitative ultrasound imaging. *Ultrason Imaging*, 17:269–290, 1995.

112. G. Luo, J. J. Kaufman, A. Chiabrera, B. Bianco, J. H. Kinney, D. Haupt, J. T. Ryaby, and R. S. Siffert. Computational methods for ultrasonic bone assessment. *Ultrasound Med Biol*, 25(5):823–830, 1999.

113. M. Maravic, C. Le Bihan, P. Landais, and P. Fardellone. Incidence and cost of osteoporotic fractures in France during 2001. A methodological approach by the national hospital database. *Osteoporos Int*, 16(12):1475–1480, 2005.

114. D. Marshall, O. Johnell, and H. Wedel. Meta-analysis of how well measures of bone mineral density predict occurrence of osteoporotic fractures. *BMJ*, 312(7041):1254–1259, 1996.

115. M. Martens, R. Van Audekercke, P. Delport, P. De Meester, and J. C. Mulier. The mechanical characteristics of cancellous bone at the upper femoral region. *J Biomech*, 16(12):971–983, 1983.

116. J. Mendlein and P. Lang. Methods and devices for improving ultrasonic measurements using anatomic landmarks and soft tissue correction. *United States Patent*, 6,013,031, 2000.

117. S. Meszaros, E. Toth, V. Ferencz, E. Csupor, E. Hosszu, and C. Horvath. Calcaneous quantitative ultrasound measurements predicts vertebral fractures in idiopathic male osteoporosis. *Joint Bone Spine*, 74(1):79–84, 2007.

118. E. Mittra, C. Rubin, B. Gruber, and Y. X. Qin. Evaluation of trabecular mechanical and microstructural properties in human calcaneal bone of advanced age using mechanical testing, microCT, and DXA. *J Biomech*, 41(2):368–375, 2008.

119. E. Mittra, C. Rubin, and Y. Qin. Interrelationship of trabecular mechanical and microstructural properties in sheep trabecular bone. *J Biomech*, 38:1229–1237, 2005.

120. H. Miwa and M. Ueda. Ultrasonic living body tissue characterization method. *United States Patent*, 4,512,195, 1985.

121. A. Morabia, A. Ross, F. Curtin, C. Pichard, and D. O. Slosman. Relation of BMI to a dual-energy X-ray absorptiometry measure of fatness. *Br J Nutr*, 82(1):49–55., 1999.

122. M. G. Mullender, S. D. Tan, L. Vico, C. Alexandre, and J. Klein-Nulend. Differences in osteocyte density and bone histomorphometry between men and women and between healthy and osteoporotic subjects. *Calcif Tissue Int*, 77(5):291–296, 2005.

123. M. Muller, P. Moilanen, E. Bossy, P. Nicholson, V. Kilappa, J. Timonen, M. Talmant, S. Cheng, and P. Laugier. Comparison of three ultrasonic axial transmission methods for bone assessment. *Ultrasound Med Biol*, 31(5):633–642, 2005.

124. E. Nägele, V. Kuhn, H. Vogt, T. Link, R. Muller, E. Lochmuller, and F. Eckstein. Technical considerations for microstructural analysis of human trabecular bone from specimens excised from various skeletal sites. *Calcif Tissue Int*, 75:15–22, 2004.

125. P. Nicholson and M. Bouxsein. Bone marrow influences quantitative ultrasound measurements in human cancellous bone. *Ultrasound Med Biol*, 28(3):369–375, 2002.

126. P. H. Nicholson and R. Alkalay. Quantitative ultrasound predicts bone mineral density and failure load in human lumbar vertebrae. *Clin Biomech (Bristol, Avon)*, 22(6):623–629, 2007.

127. P. H. Nicholson, X. G. Cheng, G. Lowet, S. Boonen, M. W. Davie, J. Dequeker, and G. Van der Perre. Structural and material mechanical properties of human vertebral cancellous bone. *Med Eng Phys*, 19(8):729–737, 1997.

128. P. H. Nicholson, G. Lowet, C. M. Langton, J. Dequeker, and G. Van der Perre. A comparison of time-domain and frequency-domain approaches to ultrasonic velocity measurement in trabecular bone. *Phys Med Biol*, 41(11):2421–2435, 1996.

129. P. H. Nicholson, R. Muller, G. Lowet, X. G. Cheng, T. Hildebrand, P. Ruegsegger, G. van der Perre, J. Dequeker, and S. Boonen. Do quantitative ultrasound measurements reflect structure independently of density in human vertebral cancellous bone? *Bone*, 23(5):425–431, 1998.

130. P. H. Nicholson, R. Strelitzki, R. O. Cleveland, and M. L. Bouxsein. Scattering of ultrasound in cancellous bone: predictions from a theoretical model. *J Biomech*, 33(4):503–506, 2000.

131. C. F. Njeh, C. M. Boivin, and C. M. Langton. The role of ultrasound in the assessment of osteoporosis: a review. *Osteoporos Int*, 7(1):7–22, 1997.

132. C. F. Njeh, T. Fuerst, E. Diessel, and H. K. Genant. Is quantitative ultrasound dependent on bone structure? a reflection. *Osteoporos Int*, 12(1):1–15, 2001.

133. C. F. Njeh, D. Hans, T. Fuerst, C. C. Glüer, and H. K. Genant, editors. *Quantitative ultrasound: Assessment of osteoporosis and bone status*. Martin Dunitz Ltd, London, 1999.

134. C. F. Njeh, D. Hans, J. Li, B. Fan, T. Fuerst, Y. Q. He, E. Tsuda-Futami, Y. Lu, C. Y. Wu, and H. K. Genant. Comparison of six calcaneal quantitative ultrasound devices: precision and hip fracture discrimination. *Osteoporos Int*, 11(12):1051–1062, 2000.

135. A. Odgaard. Three-dimensional methods for quantification of cancellous bone architecture. *Bone*, 20(4):315–328, 1997.

136. M. O'Donnell and J. G. Miller. Quantitative broadband ultrasonic backscatter. An approach to nondestructive evaluation in acoustically inhomogeneous materials. *J Appl Phys*, 52(2):1056–1065, 1981.

137. M. L. Oelze and W. D. O'Brien Jr. Frequency-dependent attenuation-compensation functions for ultrasonic signals backscattered from random media. *J Acoust Soc Am*, 111(5 Pt 1):2308–2319, 2002.

138. F. Padilla, L. Akrout, S. Kolta, C. Latremouille, C. Roux, and P. Laugier. In vitro ultrasound measurement at the human femur. *Calcif Tissue Int*, 75(5):421–430, 2004.

139. F. Padilla, E. Bossy, G. Haiat, F. Jenson, and P. Laugier. Numerical simulation of wave propagation in cancellous bone. *Ultrasonics*, 44 Suppl 1:e239–243, 2006.

140. F. Padilla, F. Jenson, and P. Laugier. Influence of the precision of spectral backscatter measurements on the estimation of scatterers size in cancellous bone. *Ultrasonics*, 44 Suppl 1:e57–60, 2006.

141. A. Parfitt. Osteonal and hemi-osteonal remodelling: the spatial and temporal framework for signal traffic in adult human bone. *J Cell Biochem*, 55(3):273–286, 1994.

142. A. Parfitt, M. Drezner, F. Glorieux, J. Kanis, H. Malluche, P. J. Meunier, S. Ott, and R. Recker. Bone histomorphometry: standardization of nomenclature, symbols and units. *J Bone Miner Res*, 2(6):595–610, 1987.

143. P. Piscitelli, G. Iolascon, F. Gimigliano, M. Muratore, P. Camboa, O. Borgia, B. Forcina, F. Fitto, V. Robaud, G. Termini, G. B. Rini, E. Gianicolo, A. Faino, M. Rossini, S. Adami, A. Angeli, A. Distante, S. Gatto, R. Gimigliano, and G. Guida. Incidence and costs of hip fractures compared to acute myocardial infarction in the Italian population: a 4-year survey. *Osteoporos Int*, 18(2):211–219, 2007.

144. L. Pothuaud, P. Carceller, and D. Hans. Correlations between gray-level variations in 2D projection images (TBS) and 3D microarchitecture: Applications in the study of human trabecular bone microarchitecture. *Bone*, 42(4):775–787, 2008.

145. K. Raum, I. Leguerney, F. Chandelier, E. Bossy, M. Talmant, A. Saied, F. Peyrin, and P. Laugier. Bone microstructure and elastic tissue properties are reflected in QUS axial transmission measurements. *Ultrasound Med Biol*, 31(9):1225–1235, 2005.

146. P. J. Roughley, R. J. White, M. C. Magny, J. Liu, R. H. Pearce, and J. S. Mort. Non-proteoglycan forms of biglycan increase with age in human articular cartilage. *Biochem J*, 295(2):421–426, 1993.

147. M. D. Rousculp, S. R. Long, S. Wang, M. J. Schoenfeld, and E. S. Meadows. Economic burden of osteoporosis-related fractures in medicaid. *Value Health*, 10(2):144–152, 2007.

148. C. Roux, V. Roberjot, R. Porcher, S. Kolta, M. Dougados, and P. Laugier. Ultrasonic backscatter and transmission parameters at the os calcis in postmenopausal osteoporosis. *J Bone Miner Res*, 16(7):1353–1362, 2001.

149. M. Rupprecht, P. Pogoda, M. Mumme, J. Rueger, K. Puschel, and M. Amling. Bone microarchitecture of the calcaneus and its changes in aging: A histomorphometric analysis of 60 human specimens. *J Orthop Res*, 24(4):664–674, 2006.

150. A. Sarvazyan and A. Tatarinov. Method and device for multiparametric ultrasonic assessment of bone conditions. *United States Patent*, 6,468,215B1, 2002.

151. C. Schoenfeld, E. Lautenschlager, and P. Meyer. Mechanical properties of human cancellous bone in the femoral head. *Med Biol Eng Comput*, 12(3):313–317, 1974.

152. N. Sebaa, Z. E. Fellah, M. Fellah, E. Ogam, A. Wirgin, F. G. Mitri, C. Depollier, and W. Lauriks. Ultrasonic characterization of human cancellous bone using the Biot theory: inverse problem. *J Acoust Soc Am*, 120(4):1816–1824, 2006.

153. S. Shahtaheri. The microanatomy of trabecular bone in young normal and osteoporotic elderly males. *Aging Male*, 10(2):71–75, 2007.

154. S. Simon. *Orthopaedic basic science*. American academy of orthopaedic surgeons, 1994.

155. T. J. Sims, N. C. Avery, and A. J. Bailey. Quantitative determination of collagen crosslinks. *Methods Mol Biol*, 139:11–26, 2000.

156. A. Stevens and J. Lowe. *Human histology*. Mosby, London, 2 edition, 1997.

157. K. L. Stone, D. G. Seeley, L. Y. Lui, J. A. Cauley, K. Ensrud, W. S. Browner, M. C. Nevitt, and S. R. Cummings. BMD at multiple sites and risk of fracture of multiple types: long-term results from the Study of Osteoporotic Fractures. *J Bone Miner Res*, 18(11):1947–1954, 2003.

158. B. Tao, J. Liu, X. Li, J. Wang, W. Wang, and G. Ning. An assessment of the use of quantitative ultrasound and the osteoporosis self-assessment tool for asians in determining the risk of nonvertebral fracture in postmenopausal chinese women. *J Bone Miner Metab*, 26(1):60–65, 2008.

159. U. Tarantino, G. Cannata, D. Lecce, M. Celi, I. Cerocchi, and R. Iundusi. Incidence of fragility fractures. *Aging Clin Exp Res*, 19(4 Suppl):7–11, 2007.

160. P. Townsend, P. Raux, R. Rose, R. Miegel, and E. Radin. The distribution and anisotropy of the stiffness of cancellous bone in the human patella. *J Biomech*, 8(6):363–367, 1975.

161. C. Turner and D. Burr. Basic biomechanical measurements of bone: A tutorial. *Bone*, 14:595–606, 1993.

162. J. Töyräs, H. Kröger, and J. S. Jurvelin. Bone properties as estimated by mineral density, ultrasound attenuation and velocity. *Bone*, 25(6):725–731, 1999.

163. J. P. Van den Bergh, C. Noordam, A. Ozyilmaz, A. R. Hermus, A. G. Smals, and B. J. Otten. Calcaneal ultrasound imaging in healthy children and adolescents: relation of the ultrasound parameters BUA and SOS to age, body weight, height, foot dimensions and pubertal stage. *Osteoporos Int*, 11(11):967–976, 2000.

164. J. P. Van den Bergh, C. Noordam, J. Thijssen, J. Otten, A. Smals, and A. Hermus. Measuring skeletal changes with calcaneal ultrasound imaging in healthy children and adults: the influence of size and location of the region of interest. *Osteoporos Int*, 12:970–979, 2001.

165. S. Viguet-Carrin, P. Garnero, and P. D. Delmas. The role of collagen in bone strength. *Osteoporos Int*, 17:319–336, 2006.

166. J. H. Waarsing, J. S. Day, and H. Weinans. An improved segmentation method for in vivo microCT imaging. *J Bone Miner Res*, 19(10):1640–1650, 2004.

167. R. Waddington, H. Roberts, R. Sugars, and E. Schönherr. Differential roles for small leucine-rich proteoglycans in bone formation. *Eur Cell Mater*, 6(6):12–21, 2003.

168. X. Wang, R. A. Bank, J. M. TeKoppele, and C. M. Agrawal. The role of collagen in determining bone mechanical properties. *J Orthop Res*, 19:1021–1026, 2001.

169. K. A. Wear. Frequency dependence of ultrasonic backscatter from human trabecular bone: theory and experiment. *J Acoust Soc Am*, 106(6):3659–3664, 1999.

170. K. A. Wear. Anisotropy of ultrasonic backscatter and attenuation from human calcaneus: implications for relative roles of absorption and scattering in determining attenuation. *J Acoust Soc Am*, 107(6):3474–3479, 2000.

171. K. A. Wear. A stratified model to predict dispersion in trabecular bone. *IEEE Trans Ultrason Ferroelectr Freq Control*, 48(4):1079–1083, 2001.

172. K. A. Wear. Autocorrelation and cepstral methods for measurement of tibial cortical thickness. *IEEE Trans Ultrason Ferroelectr Freq Control*, 50(6):655–660, 2003.

173. K. A. Wear. The effect of phase cancellation on estimates of broadband ultrasound attenuation and backscatter coefficient in human calcaneus in vitro. *IEEE Trans Ultrason Ferroelectr Freq Control*, 55(2):384–390, 2008.

174. K. A. Wear and r. Armstrong, D. W. Relationships among calcaneal backscatter, attenuation, sound speed, hip bone mineral density, and age in normal adult women. *J Acoust Soc Am*, 110(1):573–578, 2001.

175. K. A. Wear and B. S. Garra. Assessment of bone density using ultrasonic backscatter. *Ultrasound Med Biol*, 24(5):689–695., 1998.

176. K. A. Wear and A. Laib. The dependence of ultrasonic backscatter on trabecular thickness in human calcaneus: theoretical and experimental results. *IEEE Trans Ultrason Ferroelectr Freq Control*, 50(8):979–986, 2003.

177. K. A. Wear, A. Laib, A. P. Stuber, and J. C. Reynolds. Comparison of measurements of phase velocity in human calcaneus to Biot theory. *J Acoust Soc Am*, 117(5):3319–3324, 2005.

178. K. A. Wear, A. P. Stuber, and J. C. Reynolds. Relationships of ultrasonic backscatter with ultrasonic attenuation, sound speed and bone mineral density in human calcaneus. *Ultrasound Med Biol*, 26(8):1311–1316, 2000.

179. J. Weaver and J. Chalmers. Cancellous bone: Its strength and changes with aging and an evaluation of some methods for measuring its mineral content. *J Bone Joint Surg Am*, 48:289–299, 1966.

180. P. N. T. Wells. *Physical Principles of Ultrasonic Diagnosis*. Academic Press, London, 1969.

181. P. N. T. Wells. *Biomedical Ultrasonics*. Academic Press, London, 1977.

182. J. Wolff. Das gestez der tranformation der knochen. *Hirschwald, Berlin*, 1892.

183. C. Y. Wu, C. C. Gluer, M. Jergas, E. Bendavid, and H. K. Genant. The impact of bone size on broadband ultrasound attenuation. *Bone*, 16(1):137–141, 1995.

184. M. Yanagiura, A. Watanabe, S. Yamada, and M. Nakajima. Ultrasonic biotissue measuring apparatus and ultrasonic biotissue measuring method. *Japan Patent*, 2001128973A, 2001.

185. M. Yanagiura, S. Yamada, M. Nakajima, and A. Watanabe. Ultrasonic living body tissue measuring method and ultrasonic living body tissue measuring device. *Japan Patent*, 2000237189A, 2000.

186. H. S. Yoon and J. L. Katz. Ultrasonic wave propagation in human cortical bone-i. theoretical considerations for hexagonal symmetry. *J Biomech*, 9(6):407–412, 1976.

ORIGINAL PUBLICATIONS

Kuopio University Publications C. Natural and Environmental Sciences

C 218. Madetoja, Elina. Novel process line approach for model-based optimization in papermaking.
2007. 125 p. Acad. Diss.

C 219. Hyttinen, Marko. Formation of organic compounds and subsequent emissions from
ventilation filters.
2007. 80 p. Acad. Diss.

C 220. Plumed-Ferrer, Carmen. Lactobacillus plantarum: from application to protein expression.
2007. 60 p. Acad. Diss.

C 221. Saavalainen, Katri. Evaluation of the mechanisms of gene regulation on the chromatin
level at the example of human hyaluronan synthase 2 and cyclin C genes.
2007. 102 p. Acad. Diss.

C 222. Koponen, Hannu T. Production of nitrous oxide (N_2O) and nitric oxide (NO) in boreal
agricultural soils at low temperature.
2007. 102 p. Acad. Diss.

C 223. Korkea-aho, Tiina. Epidermal papillomatosis in roach (Rutilus rutilus) as an indicator of
environmental stressors.
2007. 53 p. Acad. Diss.

C 224. Räisänen, Jouni. Fourier transform infrared (FTIR) spectroscopy for monitoring of solvent
emission rates from industrial processes.
2007. 75 p. Acad. Diss.

C 225. Nissinen, Anne. Towards ecological control of carrot psyllid (Trioza apicalis).
2008. 128 p. Acad. Diss.

C 226. Huttunen, Janne. Approximation and modellingerrors in nonstationary inverse problems.
2008. 56 p. Acad. Diss.

C 227. Freiwald, Vera. Does elevated ozone predispose northern deciduous tree species to abiotic
and biotic stresses?
2008. 109 p. Acad. Diss.

C 228. Semenov, Dmitry. Distance sensing with dynamic speckles.
2008. 63 p. Acad. Diss.

C 229. Höytö, Anne. Cellular responses to mobile phone radiation: proliferation, cell death and
related effects.
2008. 102 p. Acad. Diss.

C 230. Hukkanen, Anne. Chemically induced resistance in strawberry (Fragaria × ananassa) and
arctic bramble (Rubus arcticus): biochemical responses and efficacy against powdery mildew and
downy mildew diseases.
2008. 98 p. Acad. Diss.

C 231. Hanhineva, Kati. Metabolic engineering of phenolic biosynthesis pathway and metabolite
profiling of strawberry (Fragaria × ananassa).
2008. 80 p. Acad. Diss.

C 232. Nissi, Mikko. Magnetic resonance parameters in quantitative evaluation of articular cartilage:
studies on T_1 and T_2 relaxation time.
2008. 83 p. Acad. Diss.